This is the Author's [*accepted*] manuscript version of the following contribution:

Malikan, Mohammad, and Victor A. Eremeyev. "On time-dependent nonlinear dynamic response of micro-elastic solids." International Journal of Engineering Science 182 (2023): art no.103793. pagg. 1-26

The publisher's version is available at:

http://dx.doi.org/10.1016/j.ijengsci.2022.103793

When citing, please refer to the published version.

On time-dependent nonlinear dynamics of micro-elastic solids

Abstract

A new approach to the mechanical response of micro-mechanic problems is presented using the modified couple stress theory. This model captured micro-turns due to micro-particles' rotations which could be essential for microstructural materials and/or at small scales. In a micro media based on the small rotations, sub-particles can also turn except the whole domain rotation. However, this framework is competent for a static medium. In terms of dynamic investigations of micro materials, it is required to involve micro-rotations' mass inertias. This fact persuades us to pay particular attention to the micro mechanics' models and directed us to re-derive the modified couple stress model to propose and represent a new micro-mechanic approach which is well-deserved, especially for dynamic studies of microstructures. In carrying out this job, the classical beam has provided the basic form of formulation procedure. The continuum medium has been limited to a square flat non-porous beam deducing a homogeneous isotropic micromaterial. As long as the time-dependent results are concerned due to studying micro-mass inertia in time history, there would be two solution steps. The Galerkin decomposition technique is imposed in accord with an analytical postulate to issue the algebraic problem distributing time-dependent equations. The latter, the Homotopy perturbation method delivers time-dependent outcomes. The solution methods have been validated by building numerical models in Abaqus software. On the new achievements of this study, one can declare that both static and dynamic length scale parameters are very effective in order to study vibrations of microstructures. If the values of these characteristic lengths are considerable, the nonlinear frequency analysis will be essential. Furthermore, the stiffness of the structure will be higher if the values of both length scale parameters increase.

1 Introduction

The materials found at a micro-level are well-known as microstructures. Particularly, the sub-particles of these materials have been revealed within the meso and micro phases. Pores, lamellae, spherulites, dendrites, precipitates, grains, etc., in these materials, can be detected in the microphase. By the use of a range of electron or optical microscopy methods, the phases can be recognized individually based on the different amorphous, crystalline, and semi-crystalline structures. Most apparently, the material behavior and physical characteristics are affected by microstructures. It is required to build a connection among specific properties

happening at a micro level and the macroscale properties also tailor the material microstructure in order to acquire explicit and precise knowledge of the behavior of the material. What is more, while describing a material's micro properties, it is momentous to take into account a length scale for the carried-out observations. This is because while using various length scales, the microstructural characteristics of the employed material differ enormously (Zum Gahr, 1987; Malikan et al., 2020a; Stempin & Sumelka, 2022; Abdussalam Nuhu & Safaei, 2022; Chen et al., 2021; Fan et al., 2021). On this subject, some researchers have already probed that a micromaterial does not include a constant-value length scale and the value of this factor shifts with a variation in the material sizes principally its thickness (Akbarzadeh Khorshidi, 2018).

A strong pack of well-presented studies has been witnessed by the literature in order to predict the mechanical behavior of microscale beam/plate-like materials on the grounds of the couple stress (Anthoine, 2000; Mindlin, 1963; Toupin, 1962; Yang et al., 2002; Yang et al., 2021; Safaei, 2021; Lu et al., 2021) and the modified couple stress models (Arefi & Taghavian, 2022; Dastjerdi et al., 2021; Dehrouyeh-Semnani, 2021; Dehrouyeh-Semnani & Mostafaei, 2021; Jouneghani et al., 2020; Kong, 2022; Kumar Jena, 2022; Li e al., 2018; Malikan, 2017; Sedighi & Bozorgmehri, 2016; Tsiatas, 2009; Yuan et al., 2020). As far as we are focusing on the couple stress models only, we will not expand the methods performed in those works, such as beam/plate models, solution techniques, and the results they have achieved. Because these factors do not concern the scope of the present work. The originality of this research relates to the type of couple stress model. Adding to these references, there have been found some works especially attended a couple stress model for anisotropic micro materials (He et al., 2017; Ma et al., 2020; Qu et al., 2020; Thanh et al., 2019; Wang & Zheng, 2018; Yang & Chen, 2015). Very few published works on the different couple stress theories have interfered with mass micro-inertias due to micro-rotations in their formulations (Georgiadis & Velgaki, 2003; Fathalilou et al., 2014). However, their theoretical model is totally different from what is presented in this paper.

A deficiency in the popular couple stress theories, from these authors' point of view, can be the static form of the models frequently employed in the rigorous literature. This contradicts the main couple stress assumptions. In terms of static studies of microstructures, the couple stress and modified couple stress theories may be consistent. However, these theories in turn exclude the mass inertia resulting from micro-rotation. Herewith, eliminating the micro-inertias of grains will not lead to a well-modeled microstructure. In this study, a new modified couple stress model is found out composing of two sections. The first one is regarding the routine

micro-rotations. On the other hand, the second part consists of micro-mass inertia which is normally neglected in the conventional couple stress models. The primary intention of this study has been concentrated on investigating these two micro-size phases, introducing one extra length scale characteristics quantity. In the concrete, a wide range of sub-movements have been supposed by this paper.

The sections of this paper are ordered as; first, by presenting section 2 the theoretical examination is undertaken. This section, for one, includes some sub-sections taking into review a continuum medium, classic and modified couple stress approaches, and more importantly, mass micro-inertias. The next section is devoted to a physical specimen represented for giving the results on a beam-like structure all based on the Euler-Bernoulli beam theory. Afterward, by means of section 4, a solution of the derived governing equations will proceed further. The Galerkin decomposition method is applied for clamped and simple edge conditions beams, resulting in the algebraic relations which reckon bifurcation conditions. The Homotopy perturbation technique is required to solve the obtained algebraic equations which are based on the time unknown variable. Thereafter, there is a need to approve the solution method by the given literature. Results should be discussed in detail due to various essential parameters affecting the micro-beam time-dependent dynamic response. This is addressed by the use of section 6. In this part, we will see whether the new phases of micro-particles proposed in this study, will be able to affect the mechanical response of a microstructure based on several theoretical estimations. We expect that the last section grants a brief but adequate and efficient conclusion about the whole paper along with the novel results.

2 Governing equations

Let us consider the peculiarities of the proposed model. First, we consider linear elasticity.

2.1 Classic continuum model under small deformations

Deformations of a material are defined through the vector of first-order displacements (u)

$$u = u(x,t) \tag{1}$$

where x is a position vector and t is time.

The corresponding strain tensor is given by (Lai et al., 1993; Malikan & Eremeyev, 2022; Malikan et al., 2020b),

$$\varepsilon = \frac{1}{2}\left(\nabla u + \nabla u^{T}\right) \tag{2}$$

where the fourth-order elasticity tensor is demonstrated by C. Moreover, the Greek letter ∇ represents the 3D nabla operator meaning the gradient, and T means matrix transpose.

The balance of forces on any internal volume (V) with a surface (S) can be written considering the dynamics laws (Lai et al., 1993; Malikan & Eremeyev, 2022; Malikan et al., 2020b),

$$\left(\int_{V} \rho v dV\right)^{\cdot} = \int_{S} T_{(n)} dS + \int_{V} \rho F dV \tag{3}$$

in which $v = \dot{u}$, and F reveals the external volumetric loads. Further, $()^{\cdot}$ exhibits derivate regarding time, and ρ shows the mass density. $T_{(n)}$ denotes a surface traction vector defined through symmetric Cauchy stress tensor σ.

Also, surface traction is expressed as (Lai et al., 1993; Malikan & Eremeyev, 2022; Malikan et al., 2020b),

$$T_{(n)} = n.\sigma \tag{4}$$

For an isotropic solid the components of σ are given by

$$\sigma_{ij} = \lambda \varepsilon_{kk} \delta_{ij} + 2G\varepsilon_{ij} \tag{5}$$

where λ and G are Lame elastic moduli, δ_{ij} is the Kronecker symbol.

Governing equations of dynamics could be derived using Hamilton's principle

$$\left(\int_{V} \delta K dV = \int_{V} \delta U dV - \delta W\right)\Bigg|_{t_{1}}^{t_{2}} \tag{6}$$

where W denotes the works of external forces, given by

$$\delta W = \int_{V} F \cdot \delta u dV + \int_{\partial V} T.\delta u dS \tag{7}$$

U and *K* determine the strain energy density and the kinetic energy density, respectively. In Eq. (7) *T* is a surface loading vector, the dot stands for a scalar product, and δu is a variation of displacements.

2.2 Classical couple stress theory

Couple stress theory can be idiomatically named as a child of Cosserat elasticity theory. Indeed, it is a simplified and shortened form of the Cosserat brothers' model. The standard and classical form of couple stress theory has been developed by Mindlin, (1963).

As a principal definition of Cauchy couple stress tensor, one can say that there exists a tensor μ upon a unit surface with normality *n* if a torque (couple) $M_{(n)}$ is acting on the surface (Grekova, 2019; Eringen, 1999; Hadjesfandiari & Dargush, 2015; Mindlin & Tiersten, 1962),

$$M_{(n)} = n.\mu \tag{8}$$

The couple stress tensor (μ) itself does not depend on the *n*. If in an actual configuration one defines the gradient of angular velocity as $\nabla\omega$, couple stress tensor works on this gradient. However, in contrast, stress tensor σ works on the translational velocity' gradient (∇v) in the same structure.

In continuing with the micro-medium and when the heat effects are absent, the balance of energy would be written as (Grekova, 2019, Eringen, 1999;),

$$\left(\int_V \rho\left(K_\mu + U\right)\delta V\right)^{\cdot} = \int_S \left(T_{(n)}.v + M_{(n)}.\omega\right)dS + \int_V \rho\left(F.v + L.\omega\right)\delta V \tag{9}$$

where *L* is the density of the external volumetric torque. The strain energy density is dependent on how the medium deforms. The kinetic energy mass density is given by the formula,

$$K_\mu = \frac{v^2}{2} + \frac{\omega.I.\omega}{2} \tag{10}$$

In (9) *I* is a symmetric microinertia tensor.

The first variation of potential energy can be written as follows (Mindlin & Tiersten, 1962; Yuan et al., 2020),

$$\delta U = \iiint_V \left(\sigma : \delta \varepsilon + \mu : \delta \chi \right) dV \tag{11}$$

where stress and couple stress constitutive relations are given by Eq. (5) and the new constitutive relation for the couple stress tensor

$$\mu_{ij} = 4l_{sr}^2 G \chi_{ij} \tag{12}$$

where l_{sr} is a static characteristic length. Let us define the asymmetric curvature (χ_{ij}) and symmetric strain (ε_{ij}) tensors aforesaid in the above equations as (Mindlin & Tiersten, 1962; Yuan et al., 2020),

$$\chi_{ij} = \frac{1}{2}\theta_{i,j} \tag{13}$$

$$\varepsilon_{ij} = \frac{1}{2}\left(u_{i,j} + u_{j,i} + u_{k,i}u_{k,j} \right) \tag{14}$$

in which u_i shows the displacements field of the domain.

The rotation vector can be calculated as,

$$\theta_i = \frac{1}{2}e_{ijk}u_{k,j} \tag{15}$$

in which e_{ijk} is the permutation symbol.

2.3 Modified couple stress theory

An altered couple stress model has been proposed by Yang and Chen (2015) in which unlike the standard form of couple stress theory, the gradient of the rotation's part is symmetric. This revised model is called the modified couple stress theory and has been used broadly and heavily so far (Arefi & Taghavian, 2022; Dastjerdi et al., 2021; Dehrouyeh-Semnani, 2021; Dehrouyeh-Semnani & Mostafaei, 2021; Jouneghani et al., 2020; Kong, 2022; Kumar Jena, 2022; Li e al., 2018; Malikan, 2017; Sedighi & Bozorgmehri, 2016; Tsiatas, 2009; Yuan et al., 2020).

The media particles' micro-rotations in the Cosserat elastic solid can be curled by the following relation,

$$\theta = \frac{1}{2}\nabla \times u \tag{16}$$
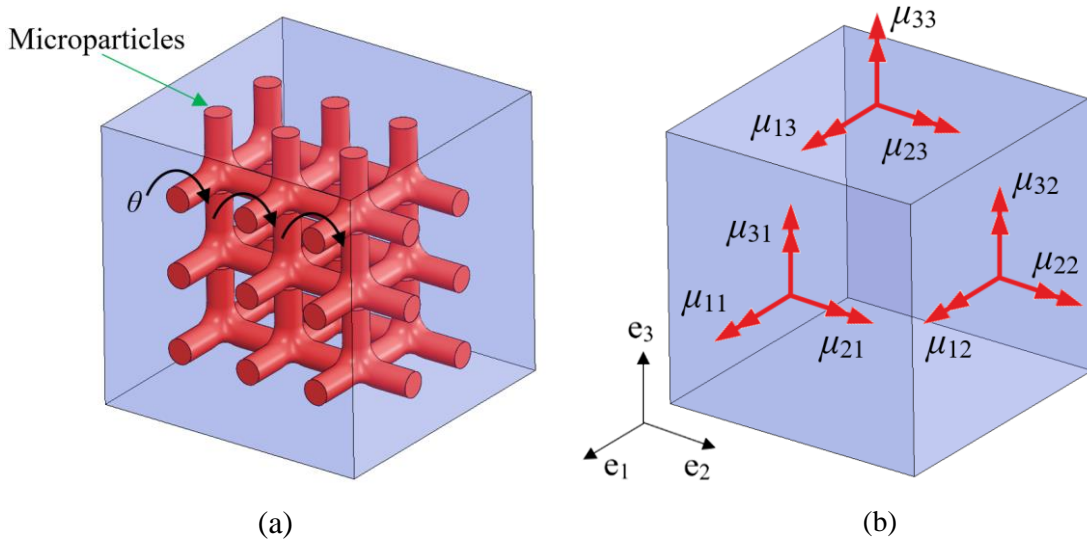
The symmetric curvature tensor can be written by

$$\chi = \frac{1}{2}\left(\nabla\theta + \nabla\theta^T\right)$$ (17)

And the stress and couple stress tensors are given by

$$\mu = 2l_{sr}^2 G\chi$$ (18)

$$\sigma = \lambda\varepsilon^T I + 2G\varepsilon$$ (19)

The micro-particles and the couple stress tensor can be graphically indicated in Fig. 1.

(a)   (b)

Fig. 1 (a) micro rotations in microscale framework (b) couple stresses in continuum medium

2.4 A dynamic extension of the modified couple stress theory

The general Cosserat micropolar theory and its sub-theories (couple stress models), as indicated briefly in the previous sections, suit the static problems and omit time-dependent at the microscale. Micro-rotations of particles inside a microstructure are still mass-dependent points and their rotation will certainly incorporate mass inertia.

The classic relation of kinetic energy can be reported by,

$$K_1 = \frac{1}{2}\int \rho(z)\sum_{i=1}^{3}\left(\frac{\partial u_i}{\partial t}\right)^2 dV$$ (20)

We here grant that the mass inertia due to the micro-rotation of the point's bodies exists in the couple stress models. Fulfilling this assumption can be possible by proposing a kinetic energy characteristic relation consisting of micro velocities by integrating the velocity of the micro-rotations as $\omega = \dot{\theta}$ inside the kinetic energy of the medium,

$$\Delta K = K_1 + \frac{1}{2} \int \rho(z) \sum_{i=1}^{3} \left[l_{dr}^2 \left(\frac{\partial \theta_i}{\partial t} \right)^2 \right] dV \tag{21}$$

in which l_{dr} is a dynamic length characteristic and credits the infinitesimal mass inertia which is deduced to exist due to micro rotations in a microstructure.

3 A physical example: a microbeam

Here we are supposed to model a beam-like microstructure as denoted by Fig. 2 for which the nonlinear natural frequencies will be calculated. The dimensions of the drawn beam are inserted into a rectangular coordinate system. The dedicated letter L is called the effective length. The lateral dimension is named thickness signed with the letter h used inside mathematical formulations.
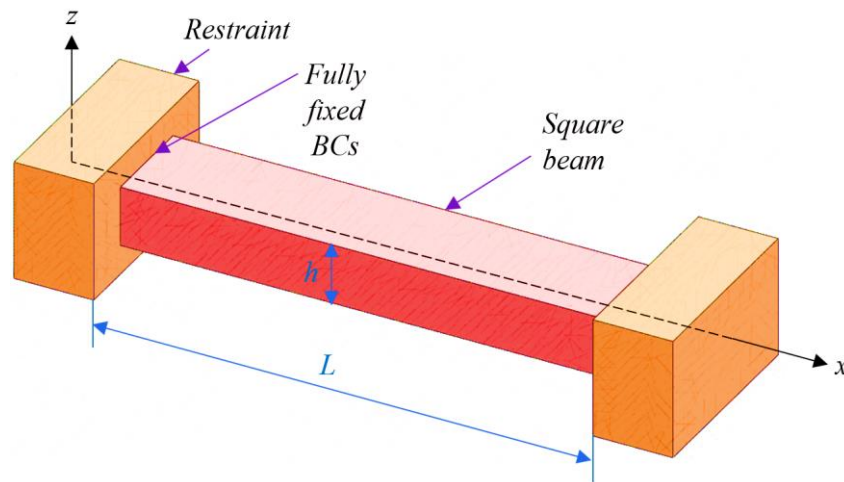
Fig. 2 A schematic continuum micro-beam fully clamped at ends

Let us here shift the 3D relations to the 1D ones on the basis of the plane strain hypothesis by means of the Euler-Bernoulli kinematic theory as follows (Barretta et al., 2022; Chen et al., 2020; Darban et al., 2022; Darban et al., 2020; Russillo et al., 2021; Russillo et al., 2022)

$$u_1(x,z,t) = u(x,t) - z\frac{\partial w(x,t)}{\partial x} \tag{22}$$

$$u_3(x,z,t) = w(x,t) \tag{23}$$

In the above-written relation, u and w are defined for the axial and transverse displacement of the mid-plane, z is the thickness variable parameter. Afterward, it is time to expand the governing equations consisting of stress and couple stress resultants in the following.

3.1 Static part

Involving Eqs. (22) and (23) allows transform the axial strain in Eq. (2) as follows

$$\{\varepsilon_{xx}\} = \frac{1}{2}\left\{2\frac{\partial u_1}{\partial x} + \left(\frac{\partial u_3}{\partial x}\right)^2\right\} \tag{24}$$

Then, we got

$$\varepsilon_{xx} = \frac{\partial u}{\partial x} - z\frac{\partial^2 w}{\partial x^2} + \frac{1}{2}\left(\frac{\partial w}{\partial x}\right)^2 \tag{25}$$

Using Hooke's law for a homogeneous isotropic material, we come to

$$\sigma_{xx} = \frac{E}{1-\nu^2}\left[\frac{\partial u}{\partial x} - z\frac{\partial^2 w}{\partial x^2} + \frac{1}{2}\left(\frac{\partial w}{\partial x}\right)^2\right] \tag{26}$$

where the parameter ν depicts the Poisson's ratio. Internal forces (stress resultants) of the media can be formulated as (Karami et al., 2022)

$$\left\{\begin{matrix} N_{ij} \\ M_{ij} \end{matrix}\right\} = \int\left\{\begin{matrix} \sigma_{ij} \\ z\sigma_{ij} \end{matrix}\right\}dz \tag{27}$$

in which the parameters N_{ij} and M_{ij} are devoted to the axial and moment stress resultants, respectively. Expanding Eq. (27) requires implementing Eq. (26) which results in

$$\begin{Bmatrix} N_{xx} \\ M_{xx} \end{Bmatrix} = \begin{Bmatrix} A_{11}\left[\dfrac{\partial u}{\partial x}+\dfrac{1}{2}\left(\dfrac{\partial w}{\partial x}\right)^2\right] \\ -D_{11}\dfrac{\partial^2 w}{\partial x^2} \end{Bmatrix} \tag{28}$$

where

$$A_{11}=\frac{Eh}{1-v^2}, \quad D_{11}=\frac{E}{1-v^2}\frac{h^3}{12}.$$

The micro-rotations vectors can be derived as

$$\theta_2=-\frac{\partial w}{\partial x} \tag{29}$$

Use of the couple stress model leads to couple stress resultants established in the form

$$\{Y_{ij}\}=\int_{-h/2}^{h/2}\{\mu_{ij}\}dz \tag{30}$$

Form Eq. (30), we get

$$\begin{Bmatrix} \mu_{xy} \\ \mu_{yx} \end{Bmatrix} = \begin{Bmatrix} -2l_{sr}^2 G\dfrac{\partial^2 w}{\partial x^2} \\ \mu_{xy} \end{Bmatrix} \tag{31}$$

$$\begin{Bmatrix} Y_{xy} \\ Y_{yx} \end{Bmatrix} = \begin{Bmatrix} -B_{sr}\dfrac{\partial^2 w}{\partial x^2} \\ Y_{xy} \end{Bmatrix} \tag{32}$$

where $B_{sr}=2l_{sr}^2 Gh$. Besides, l_{sr} stands for a static length scale parameter.

Let us reword the total potential energy relation as in (Dastjerdi et al., 2022; Xu et al., 2021a; Xu et al., 2021b),

$$\delta\int_{t_1}^{t_2}\left[K+W-U\right]dt=0 \tag{33}$$

For one-dimensional case instead of Eq. (11) we attain

$$\delta U = \iiint_V \left(\sigma_{xx} \delta \varepsilon_{xx} + \mu_{xy} \delta \chi_{xy} \right) dV \tag{34}$$

or,

$$\delta U = \iiint_V \left[\sigma_{xx} \left(\frac{\partial \delta u}{\partial x} - z \frac{\partial^2 \delta w}{\partial x^2} + \frac{\partial \delta w}{\partial x} \frac{\partial w}{\partial x} \right) + m_{xy} \left(-\frac{\partial^2 \delta w}{\partial x^2} \right) \right] dV \tag{35}$$

Integrating by part from Eq. (35) leads to nonlinear static equilibrium equations including classical and micro stress resultants as follows

$$\delta u = 0 \; ; \; \frac{\partial N_{xx}}{\partial x} = 0 \tag{36}$$

$$\delta w = 0 \; ; \; -\frac{\partial^2 M_{xx}}{\partial x^2} + \frac{\partial}{\partial x} \left(N_{xx} \frac{\partial w}{\partial x} \right) - \frac{\partial^2 Y_{xy}}{\partial x^2} = 0 \tag{37}$$

Furthermore, non-classical boundary conditions can be worded as,

$$\left(N_{xx} \delta u + \frac{\partial}{\partial x} \left(M_{xx} \delta w \right) + N_{xx} \frac{\partial w}{\partial x} \delta w - \frac{\partial}{\partial x} \left(Y_{xy} \delta w \right) \right)_0^L = 0 \tag{38}$$

3.2 Dynamic part

Let us present Eq. (21) in the open state as follows,

$$K = \frac{1}{2} \int_{-h/2}^{h/2} \rho(z) \left\{ \left(\frac{\partial u_1}{\partial t} \right)^2 + \left(\frac{\partial u_3}{\partial t} \right)^2 + l_{dr}^2 \left(\frac{\partial \theta_2}{\partial t} \right)^2 \right\} dz \tag{39}$$

Then, substituting Eqs. (22), (23), and Eq. (29) into Eq. (39), we obtain

$$K = \frac{1}{2} \int_{-h/2}^{h/2} \rho(z) \left\{ \left(\frac{\partial u}{\partial t} - z \frac{\partial^2 w}{\partial x \partial t} \right)^2 + \left(\frac{\partial w}{\partial t} \right)^2 + l_{dr}^2 \left(-\frac{\partial^2 w}{\partial x \partial t} \right)^2 \right\} dz \tag{40}$$

Afterward, simplifying Eq. (40), one gets

$$\delta K = \int_{-h/2}^{h/2} \rho(z) \left\{ \left(\frac{\partial \delta u}{\partial t} - z \frac{\partial^2 \delta w}{\partial x \partial t} \right) \left(\frac{\partial u}{\partial t} - z \frac{\partial^2 w}{\partial x \partial t} \right) + \left(\frac{\partial \delta w}{\partial t} \right) \left(\frac{\partial w}{\partial t} \right) + 2 l_{dr}^2 \left(\frac{\partial^2 \delta w}{\partial x \partial t} \right) \left(\frac{\partial^2 w}{\partial x \partial t} \right) \right\} dz \tag{41}$$

It is now possible to collect all the static and dynamic terms together in a system of equations

$$\frac{\partial N_x}{\partial x} = I_0 \frac{\partial^2 u}{\partial t^2} - I_1 \frac{\partial^3 w}{\partial x \partial t^2} \qquad (42)$$

$$-\frac{\partial^2 M_{xx}}{\partial x^2} + \frac{\partial}{\partial x}\left(N_{xx}\frac{\partial w}{\partial x}\right) - \frac{\partial^2 Y_{xy}}{\partial x^2} = I_0 \frac{\partial^2 w}{\partial t^2} + I_0' \frac{\partial^4 w}{\partial x^2 \partial t^2} - I_1 \frac{\partial^3 u}{\partial x \partial t^2} + I_2 \frac{\partial^4 w}{\partial x^2 \partial t^2} \qquad (43)$$

where the macro mass moment of inertias is available (Dastjerdi et al., 2020; Shariati et al., 2021),

$$\begin{Bmatrix} I_0 \\ I_1 \\ I_2 \end{Bmatrix} = \int_{-h/2}^{h/2} \rho(z) \begin{Bmatrix} 1 \\ z \\ z^2 \end{Bmatrix} dz \qquad (44)$$

And the micro mass moment of inertia has been found as,

$$I_0' = l_{dr}^2 \int_{-h/2}^{h/2} \rho(z) dz \qquad (45)$$

If the chosen material is homogenous, so then I_1 would be eliminated (in this paper, a homogeneous material has been picked up). Some mathematical efforts are performed concerning the integration of the stretching effect in the limit of length and then proceeding with u (0) and u (L) initial conditions enables us to calculate axial normal force. Consequently, the final nonlinear frequency equation can be arranged as follows,

$$D_{11}\frac{\partial^4 w}{\partial x^4} + H_{11}\frac{\partial^2 w}{\partial x^2}\int_0^L \left(\frac{\partial w}{\partial x}\right)^2 dx + B_{sr}\frac{\partial^4 w}{\partial x^4} = I_0 \frac{\partial^2 w}{\partial t^2} + I_0' \frac{\partial^4 w}{\partial x^2 \partial t^2} + I_2 \frac{\partial^4 w}{\partial x^2 \partial t^2} \qquad (46)$$

where

$$H_{11} = \frac{A_{11}h^2}{2L} \qquad (47)$$

4 Solution process

To consider the nonlinear mathematical model with an actual physical sample, we here proceed with an analytical solution including Galerkin weighted residual method (GWRM) and the Homotopy perturbation technique.

4.1 Galerkin decomposition method

Among analytical solution methods that separate motion governing differential relations into temporal and spatial sections, the Galerkin decomposition method is a simple and accurate one by which many problems have been solved properly (Malikan & Eremeyev, 2021).

The constitutive partial differential equations that appeared in Eq. (46) can be decomposed into algebraic equations by the application of the Galerkin scheme as the next effort. First,

$$w(x,t) = \sum_{m=1}^{\infty} X_m(x) q(t) \tag{48}$$

where $q(t)$ denotes the time response of the system and depends on frequency modes as well.

Based on the Galerkin decomposition technique, one receives

$$\int_0^L R(x,t) X_m(x) dx = 0 \tag{49}$$

where R is a residue of Eq. (46) after replacing Eq. (48) inside it as,

$$R(x,t) = D_{11} \frac{\partial^4 w}{\partial x^4} + H_{11} \frac{\partial^2 w}{\partial x^2} \int_0^L \left(\frac{\partial w}{\partial x}\right)^2 dx + B_{sr} \frac{\partial^4 w}{\partial x^4} - \left(I_0 \frac{\partial^2 w}{\partial t^2} + I_0' \frac{\partial^4 w}{\partial x^2 \partial t^2} + I_2 \frac{\partial^4 w}{\partial x^2 \partial t^2}\right) \tag{50}$$

and

$$X_m(x) = \alpha_1 \sin(\lambda_m x) + \alpha_2 \sinh(\lambda_m x) - \Lambda_m\left(\alpha_3 \cos(\lambda_m x) + \alpha_4 \cosh(\lambda_m x)\right) \tag{51}$$

The trigonometric admissible shape functions which supposed to satisfy boundary conditions are shown in Table 1 (Malikan & Eremeyev, 2022). These shape functions are presented in mode number (m).

Table 1

The admissible shape functions are chosen as trigonometric functions

Boundary Conditions		α_i	λ_m	Λ_m
	SS	$\alpha_1 = 1,\ \alpha_2 = 0,$ $\alpha_3 = 0,\ \alpha_4 = 0$	$m\pi/L$	1

	CS	$\alpha_1 = 1,\ \alpha_2 = -1,$ $\alpha_3 = 1,\ \alpha_4 = -1$	$\tan \lambda_m = \tanh \lambda_m$	$\dfrac{\sin(\lambda_m L) + \sinh(\lambda_m L)}{\cos(\lambda_m L) + \cosh(\lambda_m L)}$
	CC	$\alpha_1 = 1,\ \alpha_2 = -1,$ $\alpha_3 = 1,\ \alpha_4 = -1$	$\cos \lambda_m \cosh \lambda_m = -1$	$\dfrac{\sin(\lambda_m L) - \sinh(\lambda_m L)}{\cos(\lambda_m L) - \cosh(\lambda_m L)}$

where the aforesaid comparison functions introduced in Table 1 will be able to satisfy the following boundary conditions devoted to simply supported and clamped boundary conditions,

$$
\text{SS:} \begin{cases} w(0,t) = 0,\ w(L,t) = 0 \\ M_x(0,t) = 0,\ M_x(L,t) = 0 \end{cases} \tag{52}
$$

$$
\text{CC:} \begin{cases} w(0,t) = 0,\ w(L,t) = 0 \\ \dfrac{\partial w}{\partial x}(0,t) = 0,\ \dfrac{\partial w}{\partial x}(L,t) = 0 \end{cases} \tag{53}
$$

Replacing Eq. (51) into Eq. (49)

$$
\int_0^L \left[\begin{array}{l} D_{11} \dfrac{\partial^4 w}{\partial x^4} + H_{11} \dfrac{\partial^2 w}{\partial x^2} \int_0^L \left(\dfrac{\partial w}{\partial x} \right)^2 dx + B_{sr} \dfrac{\partial^4 w}{\partial x^4} \\ - \left(I_0 \dfrac{\partial^2 w}{\partial t^2} + I_0' \dfrac{\partial^4 w}{\partial x^2 \partial t^2} + I_2 \dfrac{\partial^4 w}{\partial x^2 \partial t^2} \right) \end{array} \right] X_m(x)\, dx = 0 \tag{54}
$$

Imposing Eq. (48) on Eq. (54) gives

$$
\int_0^L \left[D_{11} \dfrac{d^4 X_m(x)}{dx^4} q(t) + H_{11} q^3(t) \dfrac{d^2 X_m(x)}{dx^2} \int_0^L \left(\dfrac{dX_m(x)}{dx} \right)^2 dx + B_{sr} \dfrac{d^4 X_m(x)}{dx^4} q(t) \right.
$$
$$
\left. - \left(I_0 X_m(x) \dfrac{d^2 q(t)}{dt^2} + I_0' \dfrac{d^2 X_m(x)}{dx^2} \dfrac{d^2 q(t)}{dt^2} + I_2 \dfrac{d^2 X_m(x)}{dx^2} \dfrac{d^2 q(t)}{dt^2} \right) \right] X_m(x)\, dx = 0 \tag{55}
$$

Simplifying Eq. (55) leads to

$$
\int_0^L \left\{ D_{11} \dfrac{d^4 X_m(x)}{dx^4} q(t) + q^3(t) H_{11} \dfrac{d^2 X_m(x)}{dx^2} \int_0^L \left(\dfrac{dX_m(x)}{dx} \right)^2 dx + B_{sr} \dfrac{d^4 X_m(x)}{dx^4} q(t) \right.
$$
$$
\left. - \left[I_0 X_m(x) + (I_0' + I_2) \dfrac{d^2 X_m(x)}{dx^2} \right] \dfrac{d^2 q(t)}{dt^2} \right\} X_m(x)\, dx = 0 \tag{56}
$$

Executing Eqs. (56) using Table 1, will convey Eqs. (56) to an algebraic time-dependent configuration. Then, having nonlinear natural frequencies is in need of a solution of the following relation,

$$\frac{d^2q(t)}{dt^2} + \lambda_1 q(t) + \lambda_2 q^3(t) = 0 \tag{57}$$

where

$$\lambda_1 = \frac{\overline{\lambda}_3}{\overline{\lambda}_0}, \ \lambda_2 = \frac{\overline{\lambda}_2}{\overline{\lambda}_0} \tag{58}$$

$$\overline{\lambda}_0 = \int_0^L \left[I_0 X_m^2(x) + (I_0' + I_2) X_m(x) \frac{d^2 X_m(x)}{dx^2} \right] dx \tag{59}$$

$$\overline{\lambda}_2 = -H_{11} \int_0^L \left(\frac{dX_m(x)}{dx} \right)^2 dx \times \int_0^L \left(X_m(x) \frac{d^2 X_m(x)}{dx^2} \right) dx = 0 \tag{60}$$

$$\overline{\lambda}_3 = \int_0^L \left[(D_{11} + B_{sr}) X_m(x) \frac{d^4 X_m(x)}{dx^4} \right] dx \tag{61}$$

Let us assume the initial conditions

$$q(0) = f, \ \frac{dq(0)}{dt} = 0 \tag{62}$$

The Galerkin decomposition method here enables us to convert the nonlinear partial differential equations (PDE) to nonlinear ordinary ones (ODE) by decomposing the equations into temporal parts. The approximate analytical processes or numerical methods can help us simply solve the decomposed nonlinear ODE system. For this paper, the Homotopy perturbation technique will be adopted because of its high precision and entirely analytical procedure.

4.2 Homotopy perturbation technique

Due to the nonlinear terms presented in Eq. (57), the symbolic solution is here generated based on the Homotopy perturbation method as follows (He et al., 1999; Sobamowo et al., 2021; Wang et al., 2012).

The Homotopy equation is introduced below by considering a Homotopy condition as $q(r, p): \Omega \times [0, L]$,

$$H(q, p) = L(q) - L(u_0) + pL(u_0) + pN(q) = 0 \tag{63}$$

Here, u_0 denotes the initial approximation, while we define N and L as nonlinear and linear terms that appeared in Eq. (57).

Let us write down the initial approximation using conditions mentioned in Eq. (62) as,

$$u_0 = f \cos(\omega t) \tag{64}$$

where f represents an amplitude of the motion.

The initial conditions of Eq. (62) can be satisfied by Eq. (64). Now, there is a possibility to readily construct the Homotopy as,

$$H(q, p) = (p - 1)\left[\frac{d^2 u_0}{dt^2} + \lambda_1 u_0\right] + \left[\frac{d^2 q}{dt^2} + \lambda_1 q\right] + p\left(\lambda_2 q^3\right) = 0, \quad p \in [0, 1, 2, \ldots] \tag{65}$$

Let us assume that Eq. (57) takes the below solution,

$$q(t) = q_0(t) + pq_1(t) + p^2 q_2(t) + \ldots \tag{66}$$

in which $q_i(t)$, $i=0,1,2,\ldots$ are terms of q which have to be determined.

If we set $p=1$ in order to process with the Homotopy method. Thus, Eq. (66) becomes

$$q(t) = \lim_{p \to 1} q(t) = \lim_{p \to 1}\left[q_0 + pq_1 + p^2 q_2 + p^3 q_3 + \ldots\right] = q_0 + q_1 + q_2 + q_3 + \ldots \tag{67}$$

Replacing Eq. (66) in Eq. (65) provides,

$$H(q, p) = \left[\frac{d^2\left(q_0 + pq_1 + p^2 q_2 + \ldots\right)}{dt^2} + \lambda_1\left(q_0 + pq_1 + p^2 q_2 + \ldots\right)\right]$$
$$+ (p - 1)\left[\frac{d^2 u_0}{dt^2} + \lambda_1 u_0\right] + p\left[\lambda_2\left(q_0 + pq_1 + p^2 q_2 + \ldots\right)^3\right] \tag{68}$$

A series of linear ODE will be gained, if one simplifies and rearranges Eq. (68) due to the similar powers of p,

Zero-order:

$$p^0 : \left[\frac{d^2 q_0}{dt^2} + \lambda_1 q_0 \right] - \left[\frac{d^2 u_0}{dt^2} + \lambda_1 u_0 \right] = 0 \tag{69}$$

With the conditions,

$$q_0(0) = f, \quad \frac{dq_0(0)}{dt} = 0 \tag{70}$$

First-order:

$$p^1 : \frac{d^2 u_0}{dt^2} + \lambda_1 u_0 + \frac{d^2 q_1}{dt^2} + \lambda_1 q_1 + \lambda_2 q_0^3 = 0 \tag{71}$$

By introducing the initial conditions below,

$$q_1(0) = 0, \quad \frac{dq_1(0)}{dt} = 0 \tag{72}$$

Second-order:

$$p^2 : \frac{d^2 q_2}{dt^2} + \lambda_1 q_2 + 3\lambda_2 q_0^2 q_1 = 0 \tag{73}$$

Using the introduced initial conditions,

$$q_2(0) = 0, \quad \frac{dq_2(0)}{dt} = 0 \tag{74}$$

The following solution can be presented for the first-order relation,

$$\left[\frac{d^2 q_0}{dt^2} + \lambda_1 q_0 \right] = \left[\frac{d^2 u_0}{dt^2} + \lambda_1 u_0 \right] \Rightarrow q_0 = u_0 \tag{75}$$

From Eq. (75), we have

$$q_0 = f \cos(\omega t) \tag{76}$$

By substituting Eq. (76) into Eq. (71) and the second derivative of Eq. (64), the first-order relation can be solved,

$$\frac{d^2q_1}{dt^2} + \lambda_1 q_1 - f\omega^2 \cos(\omega t) + \lambda_1 f \cos(\omega t) + \lambda_2 f^3 \cos^3(\omega t) = 0 \tag{77}$$

Replacing the trigonometric identities

$$\cos^3(\omega t) = \frac{3\cos(\omega t) + \cos(3\omega t)}{4} \tag{78}$$

into Eq. (77), one achieves

$$\frac{d^2q_1}{dt^2} + \lambda_1 q_1 - f\omega^2 \cos(\omega t) + \lambda_1 f \cos(\omega t) + \lambda_2 f^3 \left(\frac{3\cos(\omega t) + \cos(3\omega t)}{4} \right) = 0 \tag{79}$$

By collecting similar expressions, one gets

$$\frac{d^2q_1}{dt^2} + \lambda_1 q_1 = -\left(\lambda_1 f - f\omega^2 + \frac{3}{4}\lambda_2 f^3 \right)\cos(\omega t) - \frac{1}{4}\lambda_2 f^3 \cos(3\omega t) \tag{80}$$

Eq. (80) is a nonhomogeneous ordinary differential equation; hence, it is possible to solve it by the method of variation of constants based on an initial guess as,

$$q_1(t) = C_1(t)\cos(\lambda_1 t) + C_2(t)\sin(\lambda_1 t) \tag{81}$$

Then, there are two answers for Eq. (80), a general answer and the specific one,

$$\begin{cases} \dfrac{d^2q_1}{dt^2} + \lambda_1 q_1 = 0 \\ \dfrac{d^2q_1}{dt^2} + \lambda_1 q_1 = -\left(\lambda_1 f - f\omega^2 + \dfrac{3}{4}\lambda_2 f^3 \right)\cos(\omega t) - \dfrac{1}{4}\lambda_2 f^3 \cos(3\omega t) \end{cases} \tag{82}$$

Now, if we proceed with the method, the constants C_1 and C_2 will be gained (the procedure is available in Appendix A). Thereafter, on the basis of Eq. (72), the first term q will be derived as follows,

$$q_1(t) = \left[f\left(\lambda_1 - \omega^2 + \frac{3}{4}f^2\lambda_2 \right)\left(\frac{\lambda_1}{\omega^2 - \lambda_1^2} \right)\cos(\omega t) + \frac{f^3\lambda_2}{4}\left(\frac{\lambda_1}{9\omega^2 - \lambda_1^2} \right)\cos(3\omega t) \right]$$
$$+ \left[f\left(\lambda_1 - \omega^2 + \frac{3}{4}f^2\lambda_2 \right)\left(\frac{\lambda_1}{\lambda_1^2 - \omega^2} \right) + \frac{f^3\lambda_2}{4}\left(\frac{\lambda_1}{\lambda_1^2 - 9\omega^2} \right) \right]\cos(\lambda_1 t) \tag{83}$$

Let us have the time-dependent response of the system. To perform this, Eqs. (76) and (83) should be substituted into Eq. (66).

$$q(t) = f\cos(\omega t) + \left[\begin{array}{l} f\left(\lambda_1 - \omega^2 + \dfrac{3}{4}f^2\lambda_2 \right)\left(\dfrac{\lambda_1}{\omega^2 - \lambda_1^2} \right)\cos(\omega t) \\ + \dfrac{f^3\lambda_2}{4}\left(\dfrac{\lambda_1}{9\omega^2 - \lambda_1^2} \right)\cos(3\omega t) \end{array} \right]$$
$$+ \left[f\left(\lambda_1 - \omega^2 + \dfrac{3}{4}f^2\lambda_2 \right)\left(\dfrac{\lambda_1}{\lambda_1^2 - \omega^2} \right) + \dfrac{f^3\lambda_2}{4}\left(\dfrac{\lambda_1}{\lambda_1^2 - 9\omega^2} \right) \right]\cos(\lambda_1 t) \tag{84}$$

This is the time history response of the nonlinear natural frequency of the system using the first two terms of the right side of Eq. (66). There are two unknowns in Eq. (84), that is, ω and t. The nonlinear natural frequency can be found by eliminating the secular terms in Eq. (84). For doing this, the coefficients of $\cos(\lambda_1 t)$ shall be set to zero.

$$f\left(\lambda_1 - \omega^2 + \frac{3}{4}f^2\lambda_2 \right)\left(\frac{\lambda_1}{\lambda_1^2 - \omega^2} \right) + \frac{f^3\lambda_2}{4}\left(\frac{\lambda_1}{\lambda_1^2 - 9\omega^2} \right) = 0 \tag{85}$$

By simplifying and rearranging Eq. (85) on the basis of ω, one obtains

$$\omega^4 + \chi_1'\omega^2 + \chi_2' = 0 \tag{86}$$

where $\chi_1' = \dfrac{\chi_2}{\chi_1}$, $\chi_2' = \dfrac{\chi_3}{\chi_1}$, and $\begin{cases} \chi_1 = 36\lambda_1^3 \\ \chi_2 = -\left[36\lambda_1^4 + \lambda_1^3\left(4 + 27f^2\lambda_2 \right) + f^2\lambda_1\lambda_2 \right]. \\ \chi_3 = 4\lambda_1^4 + \lambda_1^3\lambda_2\left(3f^2 + f^3 \right) \end{cases}$

Afterward, the roots of Eq. (86) can be found easily upon the assumption $y = \omega^2$,

$$y^2 + \chi_1'y + \chi_2' = 0 \tag{87}$$

Then, a solution to the above-written quadratic equation is available. All four roots of Eq. (86) are calculated below,

$$\omega_{NL} = \pm\sqrt{\frac{-\chi_1' \pm \sqrt{\chi_1'^2 - 4\chi_2'}}{2}} \tag{88}$$

Eq. (88) cannot be a highly accurate response for Eq. (46), indeed. In order to find a higher precise nonlinear frequency upon the second term of q, it is enough to repeat the above procedure. To reach the desired accuracy, this direction and process may be continued. Not to mention that a few terms are sufficient to get suitable results and many iterations are not required.

The linear frequency can also be calculated by $\omega_L = \sqrt{\lambda_1}$.

The mathematical model will be implemented in MATLAB and MATHEMATICA and its robustness and accuracy will be displayed through the next section.

5 Validation

To check the applicability of the solution techniques, this section is prepared. The initial comparison is exhibited with the aid of the robust finite element software, namely Abaqus. This verification is performed by tabulating Tables 2-4 for linear natural frequency and classical beam model. The material and specifications required for the validation are placed beside the title of the Table. The variable parameter is selected as the slenderness ratio (L/h). The unit of natural frequency is considered as rad/s. Moreover, the differences in results of FEM and those of the present study are demonstrated in percentage by erf% (Eq. (85)). The comparison is made from a relatively thick domain up to a thin one. As observed, when the I_2 is eliminated, the present results are closer to those of Abaqus. For this part of the validation, a good agreement can be seen.

$$erf\% = \frac{|present - reference|}{reference} \times 100 \tag{89}$$

Table 2. Solution validation of linear natural frequency by means of Abaqus for a squared macro beam (E=210e3 MPa, υ= 0.3, h=10 mm, L_y=L_x, ρ=2.2 tonne/mm^3, SS)

L/h	Present with I_2 *	Present without I_2	Abaqus	Erf% for *
10	0.88389	0.88025	0.88027	0.41123
12	0.61304	0.61128	0.61128	0.28792
14	0.45005	0.44910	0.44910	0.21153
16	0.34440	0.34384	0.34384	0.16286

18	0.27202	0.27168	0.27168	0.12514
20	0.22029	0.22006	0.22006	0.10451
22	0.18202	0.18187	0.18187	0.08247
24	0.15293	0.15282	0.15282	0.07198
26	0.13029	0.13021	0.13021	0.06143
28	0.11233	0.11227	0.11227	0.05344
30	0.09785	0.09780	0.09780	0.05112
32	0.08599	0.08596	0.08596	0.03490
34	0.07617	0.07614	0.07614	0.03940
36	0.06794	0.06792	0.06792	0.02944
38	0.06097	0.06095	0.06095	0.03281
40	0.05502	0.05501	0.05501	0.01817

Table 3. Solution validation of linear natural frequency by means of Abaqus for a squared macro beam (E=210e3 MPa, v= 0.3, h=10 mm, L_y=L_x, ρ=2.2 tonne/mm^3, CC)

L/h	Present with I_2 *	Present without I_2	Abaqus	Erf% for *
10	1.98073	1.98057	1.99541	0.73568
12	1.37547	1.37540	1.38569	0.73753
14	1.01054	1.01049	1.01806	0.73866
16	0.77368	0.77366	0.77949	0.74535
18	0.61130	0.61128	0.61587	0.74204
20	0.49515	0.49514	0.49885	0.74170
22	0.40921	0.40920	0.41228	0.74464
24	0.34385	0.34384	0.34642	0.74187
26	0.29298	0.29298	0.29518	0.74530
28	0.25262	0.25262	0.25451	0.74260
30	0.22006	0.22006	0.22171	0.74421
32	0.19341	0.19341	0.19486	0.74412
34	0.17133	0.17132	0.17261	0.74155
36	0.15282	0.15282	0.15396	0.74045
38	0.13715	0.13715	0.13818	0.74540
40	0.12378	0.12378	0.12471	0.74573

Table 4. Solution validation of linear natural frequency by means of Abaqus for a squared macro beam (E=210e3 MPa, v= 0.3, h=10 mm, L_y=L_x, ρ=2.2 tonne/mm^3, CS)

L/h	Present with I_2*	Present without I_2	Abaqus	Erf% for *
10	1.37922	1.37540	1.37513	0.29742
12	0.95697	0.95513	0.95491	0.21572
14	0.70272	0.70173	0.70158	0.16249
16	0.53784	0.53726	0.53715	0.12845
18	0.42486	0.42450	0.42442	0.10367
20	0.34408	0.34384	0.34378	0.08726
22	0.28433	0.28417	0.28411	0.07743
24	0.23889	0.23878	0.23873	0.06702
26	0.20354	0.20346	0.20342	0.05899
28	0.17549	0.17543	0.17539	0.05701
30	0.15286	0.15282	0.15279	0.04581
32	0.13435	0.13431	0.13428	0.05213
34	0.11900	0.11897	0.11895	0.04203
36	0.10614	0.10612	0.10610	0.03770
38	0.09526	0.09524	0.09522	0.04200
40	0.08597	0.08596	0.08594	0.03490

Table 5. Validation for the nonlinear natural frequency with those obtained by the literature for SS

	Frequency ratio		
f	Present	(Bhashyam & Prathap, 1980)	(Abdul-Majid, 2011)
0.1	1.0011	1.0009	1.0010
0.2	1.0045	1.0037	1.0043
0.4	1.0178	1.0149	1.0170
0.6	1.0398	1.0332	1.0384
0.8	1.0697	1.0583	1.0673
1	1.1071	1.0897	1.1030

The published results in Tables 2-4 cannot be a perfect case in order to approve the whole solving methods, although the analytical boundary conditions can be corroborated.

To show further comparisons, nonlinear natural frequencies shall be compared to the literature or a reputable reference. Table 5 demonstrates a comparison of the natural frequencies of beams with geometrical nonlinear effects. The numerical results are compared in different frequency

amplitudes for simply-supported boundary conditions. Noted that the frequency ratio here and in the next sections means the ratio of the nonlinear frequency to that of linear. As seen, results indicate an acceptable accuracy, particularly for higher slenderness rations. It is significant to remind that for Table 5, we have not taken the I_2 into the mathematical model (Eq. (46)). It is also interesting to realize that while eliminating I_2, the analytical natural frequency approaches the Abaqus results led to this finding that Abaqus may not consider the second mass inertia in its FE formulation for 1D beam elements. Consequently, we will ignore it in the results section. One may say that this finding cannot be true for clamped end conditions. It is very crucial to note that the Student Edition of Abaqus has been used for comparison purposes and it is limited in the number of mesh so the fixed ends results may not be entirely precise. Moreover, the more the mesh, the lower the values of Abaqus results for this model.

6 Results and discussions

After finding a good accuracy for those boundary conditions and solution methods, let us investigate the critical parameters with detailed discussions.

Let us define and introduce some nondimensional parameters to easier provide the numerical results as follows,

$$F\_r = \frac{\omega_{NL}}{\omega_L}, \; f^* = \frac{f}{h}, \; x^* = \frac{x}{L}, \; L^* = \frac{L}{h}, \; l_{sr}^* = \frac{l_{sr}}{h}, \; l_{dr}^* = \frac{l_{dr}}{h}, \; W = \frac{w}{w_{max}}, \; t^* = t\sqrt{\frac{D_{11}}{\rho L^4}}$$

To start the discussion and results, in the beginning, we will discuss the effect of changes in static (SLS) and dynamic length scale (DLS) parameters. These two factors play a vital and main role in the mechanical response of the analyzed microstructure. The SLS parameter has been evaluated abundantly by researchers in the research background. However, the DLS parameter has been neglected in couple stress problems, especially dynamic problems based on the couple stress theory. Figures 3a, b, and c express the changes in the SLS parameter for the horizontal axis of the graphs, and Figures 4a, b, and c display the variation in the dynamic parameter on this axis. The ratio of nonlinear to linear frequency, which will be known as the frequency coefficient in this article, is placed on the vertical axis of these figures to represent the importance of nonlinear frequency with changes in static and dynamic parameters. Figures 3a-c and Figures 4a-c, figures are presented for a dedicated boundary condition one by one, which are respectively the beam with two clamp ends, the beam with the full hinge boundary

condition, and finally the beam with the clamp boundary condition on the left side and the hinge on the right support. With the help of Figures 3a, b, and c, as can be seen, by an increase in the SLS parameter, the significance of the nonlinear frequency becomes further. This higher importance will also be more visible in larger values of the DLS parameter. Although in the beam with two hinges, first, up to certain values of the static parameter, the importance of the nonlinear frequency decreases; but after a certain number, the frequency ratio increases which demonstrates the increase in the urgency of the nonlinear frequency. The key point is that the presence of both static and dynamic parameters leads to an increase in the natural frequency, both in the linear and nonlinear frequency modes, which is associated with greater stiffness of the material. But the increasing and decreasing trends in these graphs are related to the frequency ratio and it is not the case that, for example, the increase in the static parameter has led to a decrease in the stiffness of the material and the softening effect. Finally, with the aid of Figure 3c, one can see that the behavior of the beam with one end hinged and the other side completely fixed can be between the behavior of fully hinged and fully fixed beams. To complete this discussion, Figures 4a to 4c can be a confirmation of several results obtained that the larger the DLS parameter and the higher the SLS parameter values, the more the seriousness of the nonlinear frequency. It is essential to note that the slenderness ratio (ratio of length to the thickness of the beam) has been selected as 10. As the current model is derived based on the Euler-Bernoulli beam, one may say that the ratio shall be higher than 15 which is devoted to thin beams. However, we are aware of this case and the reasoning here is the fact that in large beams the problem will not be influenced by nonlinear terms as much as we expect. This result will be attained in the next diagrams.
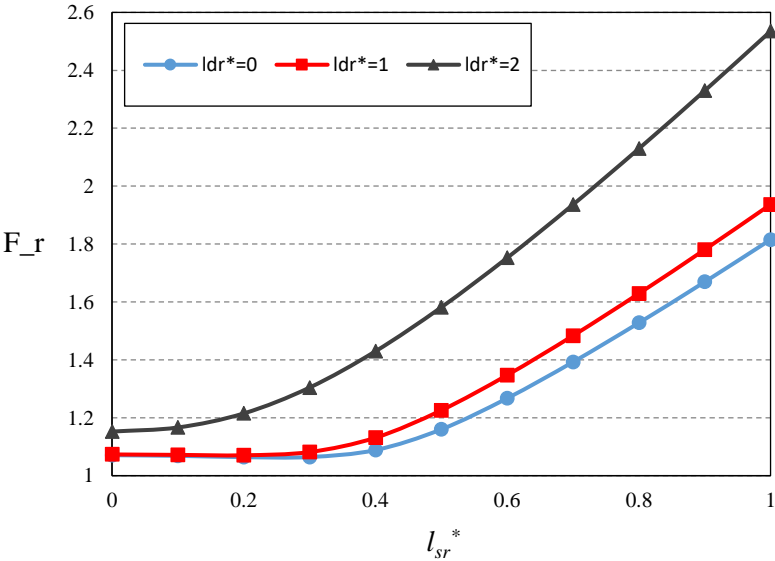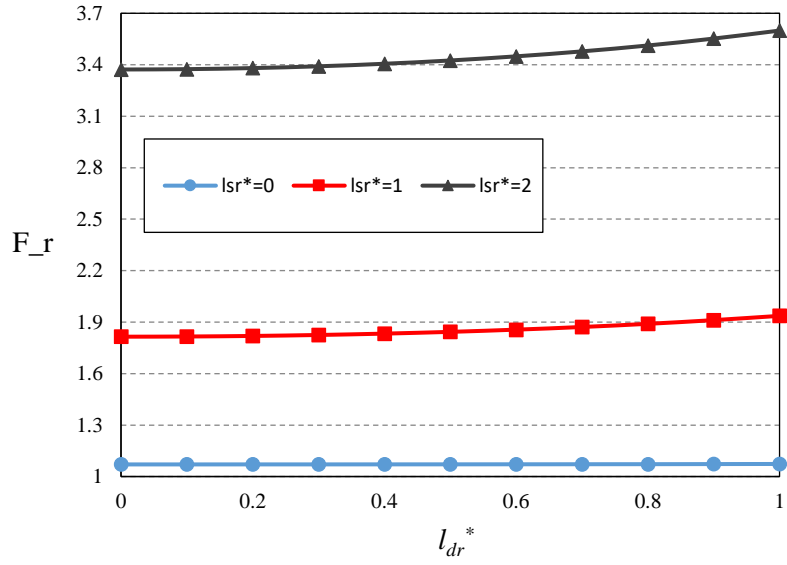
Fig 3a. Frequency ratio vs. static length scale parameter including $L^*=10$, $f^*=0.1$, CC.
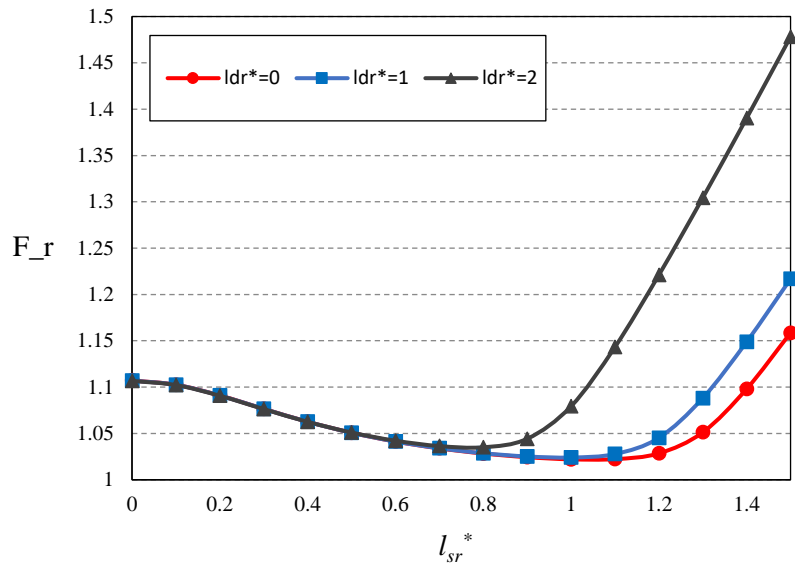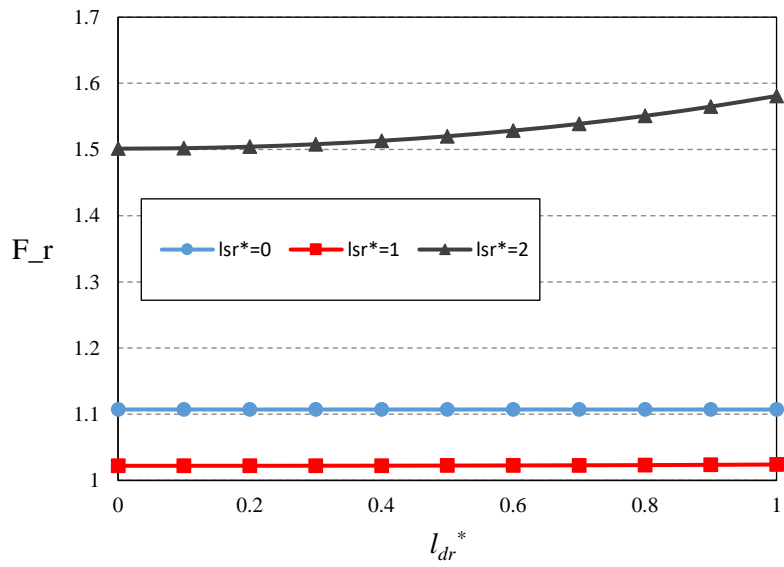

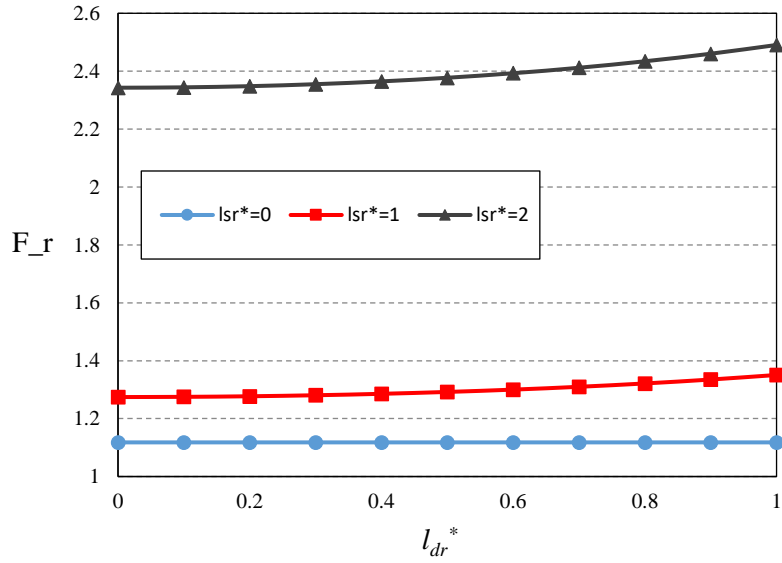**Fig 3b.** Frequency ratio vs. static length scale parameter including $L^*=10$, $f^*=0.1$, SS.
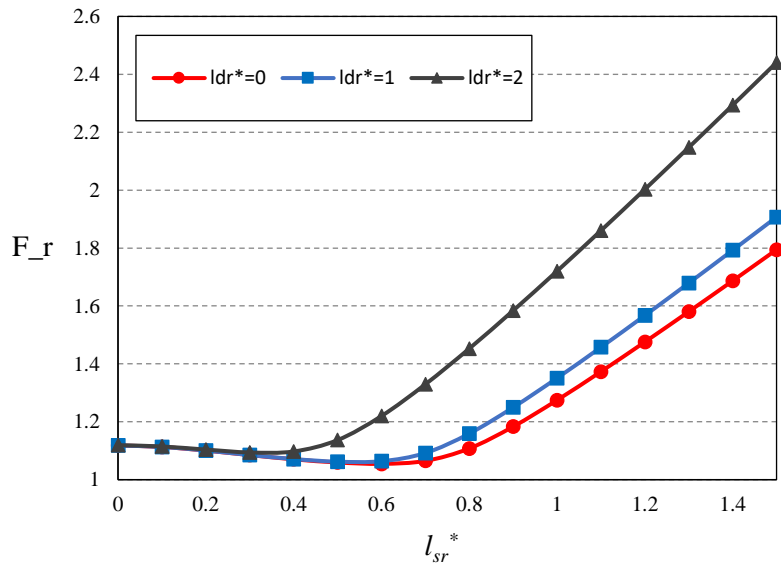
Fig 3c. Frequency ratio vs. static length scale parameter including $L^*=10$, $f^*=0.1$, CS.

Fig 4a. Frequency ratio vs. dynamic length scale parameter including $L^*=10$, $f^*=0.1$, CC.


Fig 4b. Frequency ratio vs. dynamic length scale parameter including $L^*=10$, $f^*=0.1$, SS.

Fig 4c. Frequency ratio vs. dynamic length scale parameter including $L^*=10$, $f^*=0.1$, CS.

In the study of vibration problems with large amplitudes, investigating the effect of the amplitude on the modeled beam or plate is of particular importance. In fact, since the nonlinear vibration analysis is done, we must examine the problem in the nonlinear region. By dint of Figure 5, different frequency amplitudes have been investigated and the frequency amplitude varies from linear to nonlinear states. In the figure, in one case, the SLS coefficient is fixed and the DLS one is variable. In the other case, this time the DLS parameter is constant and the SLS coefficient is changeable. It can be seen that increasing the frequency amplitude ends up increasing the nonlinear frequency effect. However, these increases will be different in the examined situations. A valuable finding that can be discussed by this figure is that the influence of a DLS parameter in the vibration problems of microstructures is very dominant and this parameter should not be simply ignored.
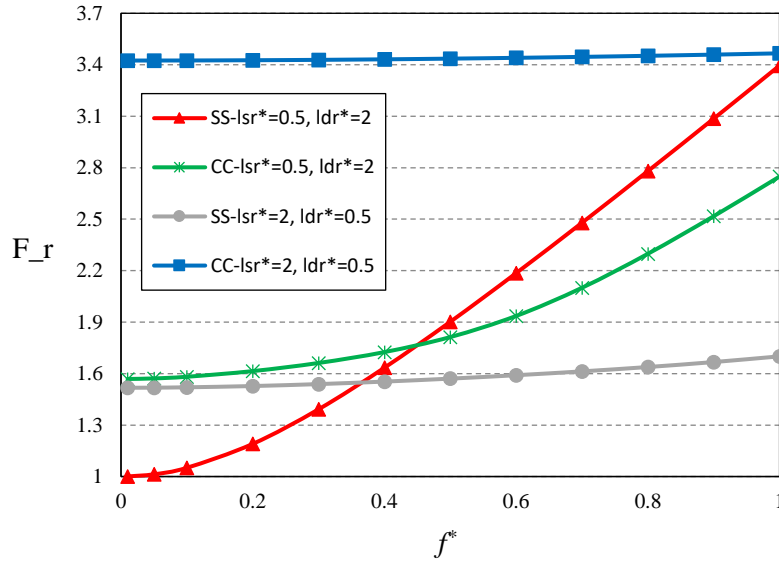
Fig 5. Frequency ratio vs. frequency amplitude
including $L^*=10$.

Beam's slenderness ratio (length to thickness) is one of the most principal factors in examining the mechanical behavior of these elements. Using Figures 6a and 6b, we evaluated the changes in slenderness coefficient from thick to thin beams in two boundary conditions in different frequency amplitudes. As can be observed, in both boundary conditions, in larger frequency ranges, the frequency ratio is a larger number which means a greater difference between the nonlinear frequency results and the linear ones. It shows that the larger the frequency amplitude, the greater the notability of the nonlinear frequency. In the hinge boundary condition, when the amplitude is small, the change in the slenderness ratio markedly influences the frequency ratio denoting that the linear frequency analysis is satisfactory to study the vibration of beams in small amplitudes. However, when the frequency range becomes higher, the slenderness ratio does not have such a noticeable effect on the variation of the frequency ratio. Moreover, in the second figure, which is related to the clamped boundary condition, it can be seen that the decrease in the frequency ratio resulting from the increase in beam slenderness has almost the same slope in all amplitudes. As another result of these two figures, it can be claimed that the beam's slenderness increases the difference between nonlinear and linear frequencies. And in fact, the longer the beam becomes, the more important the frequency amplitude will be. This result is gotten from the difference in the results of the frequency amplitudes in larger values of the slenderness coefficient. However, the effectiveness of the slenderness ratio from $L^*=10$ is insignificant in the frequency ratio.
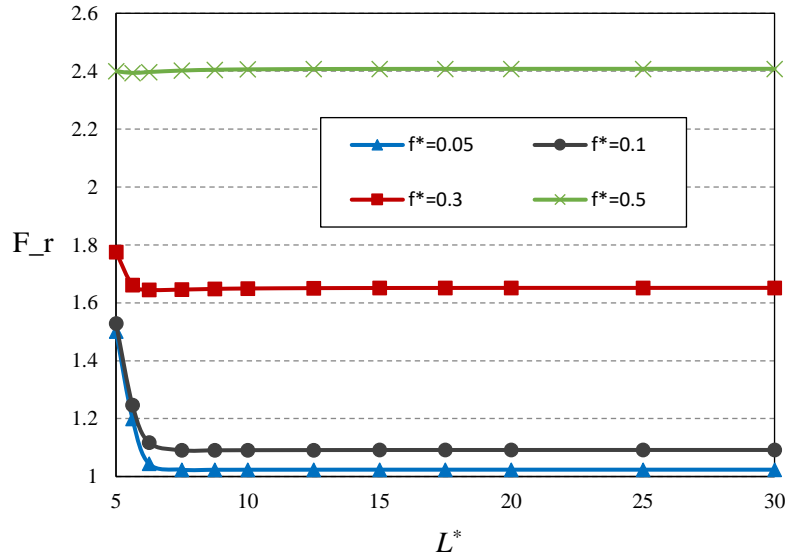
Fig 6a. Frequency ratio vs. slenderness coefficient including $l_{sr}^*=0.2$, $l_{dr}^*=0.2$, SS.
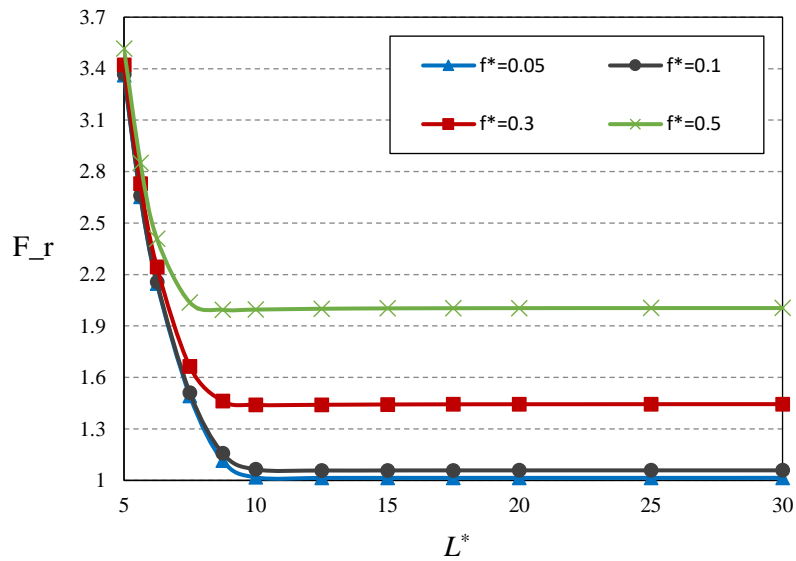

Fig 6b. Frequency ratio vs. slenderness coefficient including $l_{sr}^*=0.2$, $l_{dr}^*=0.2$, CC.

The shape of the frequency modes is almost a geometrical problem, and in small-scale beams, it can be similar to macro-scale beams, although with a difference in its dynamic transverse deflection rate. Figures 7a, b, and c were drawn to display the frequency mode shapes from the first frequency mode to the fourth one in three various boundary conditions. On the other hand, the accuracy of the trigonometric functions presented in Table 1 for the beam with three types of boundary conditions can also be confirmed here. Of course, it is necessary to remember that these mode shapes are dynamic and time-dependent. To plot them, we considered time equal to

pi. It should also be mentioned that the frequency range also affects these modes. In fact, time, frequency amplitude, and SLS and DLS parameters can differ the phase of the modes. But in order to pull out these three figures, we avoided producing the modes in a different phase state and tried to show more of the geometric aspect of the modes. The correctness of the trigonometric functions used for the analytical solution is fully confirmed by drawing these three figures.
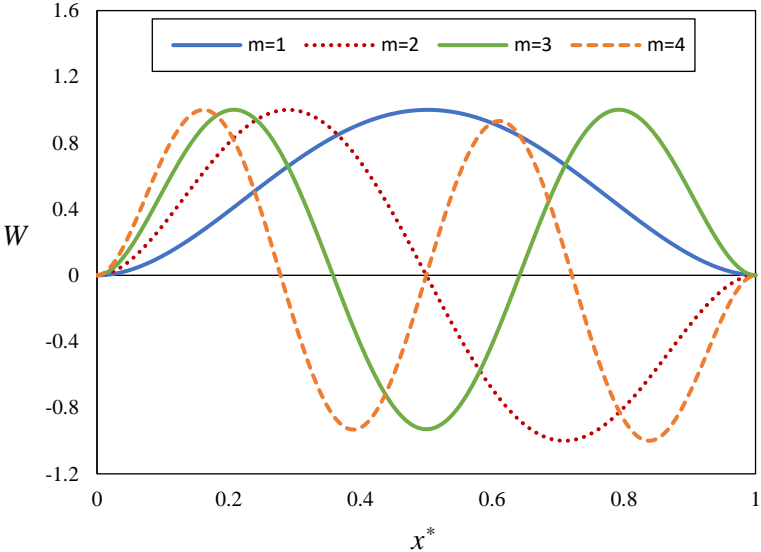
Fig 7a. Dynamic transverse displacements vs. normalized dimensionless mode shapes including l_{sr}^*=0.2, l_{dr}^*=0.2, f^*=0.1, CC.
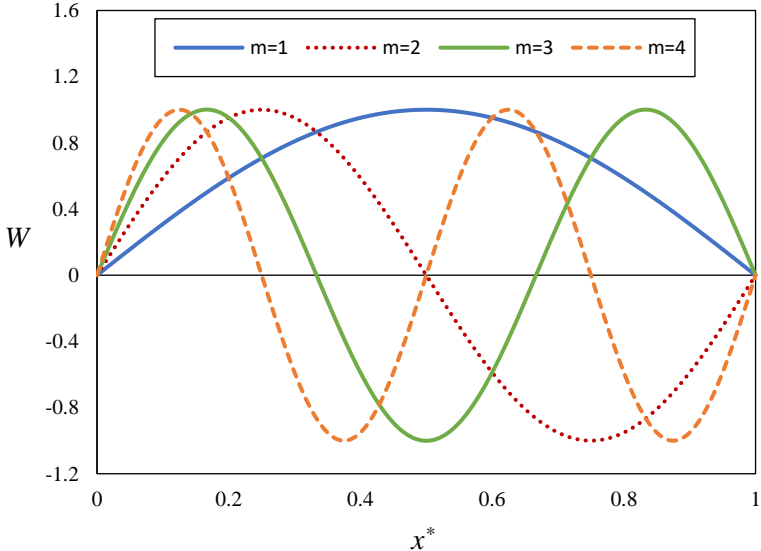

Fig 7b. Dynamic transverse displacements vs. normalized dimensionless mode shapes including l_{sr}^*=0.2, l_{dr}^*=0.2, f^*=0.1, SS.
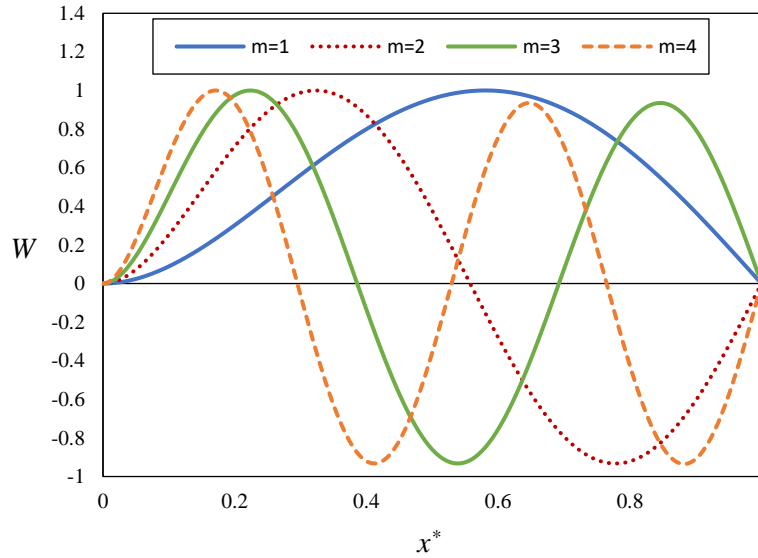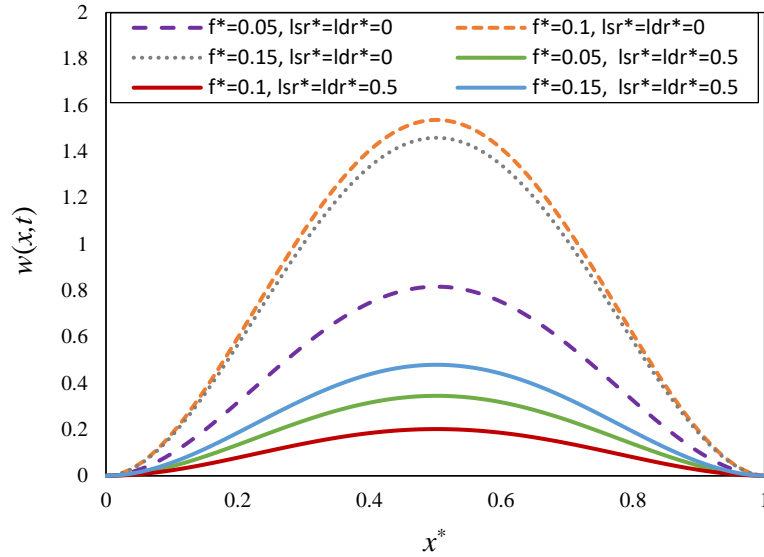
Fig 7c. Dynamic transverse displacements vs. normalized dimensionless mode shapes including l_{sr}^*=0.2, l_{dr}^*=0.2, f^*=0.1, CS.

Figures 8a and 8b are represented to study the effect of SLS and DLS parameters on dynamic deflections in two boundary conditions. The figures have been plotted in cases where the beam is without microscale effects as compared to the beam with microscale effects. The different frequency amplitude ranges have also been shown. In this problem, the phase difference has been neglected and all the deflections have been drawn as positive. These figures were also extracted at the time of pi. As it is clear, the frequency modes are in the first mode. By studying these two figures, it can be concluded that small-scale static and dynamic length scale effects should be taken into consideration in the vibration problems of microstructures because they cause serious differences in the results of transverse dynamic deflections.
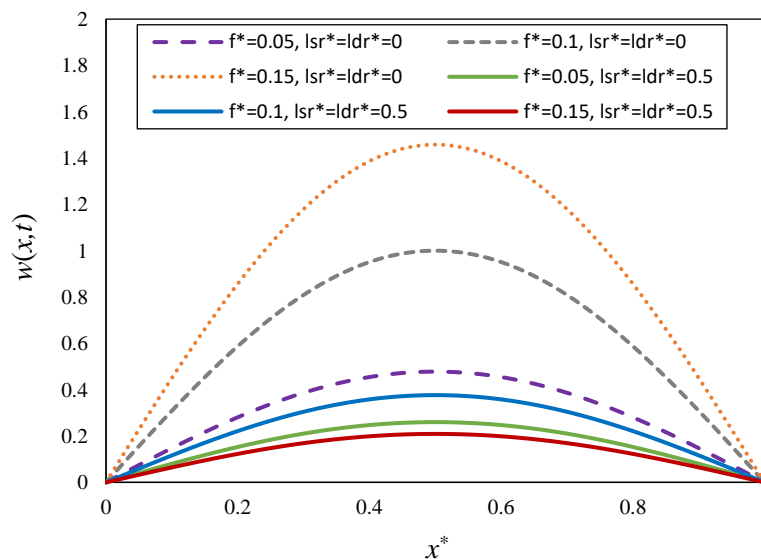
Fig 8b. Normalized mode shapes vs. frequency amplitudes

including *m*=1, CC.

After assessing the results in different situations with changes in various parameters, it is time to check the time history response of the system in different conditions. Figures 9a and 9b are plotted to exhibit the effects of large and small frequency amplitudes on the time history of the hinged beam. On the other hand, Figures 10a and 10b also illustrate the same conditions but for the beam with two fixed ends. In Figures 9a and 10a, since the amplitude is larger than that of Figures 9b and 10b, more cycles and shorter wavelengths are observed, which means that the frequency value is bigger in the larger amplitude, which is a classic result in nonlinear vibrations studies. Researchers and Engineers have already proven it. The result extracted in this research can be that the effect of the microscale leads to the phase difference in the time response of the frequency. This phase difference is not only specific to large frequency amplitudes and can be seen in small ranges as well. As a point of fact, the influence of the microscale slows down the movement of the system, and the same thing creates a phase difference in the time history of the system, which of course, is clear and evident as time increases. This phase difference will increase until it reaches a difference of 2pi. Another valuable result of these figures can be mentioned in Figure 10a. When the frequency amplitude is large in the beams of the double-fixed, the shape of the time response of the system will entirely change and it will leave the harmonic state with a smooth and uniform curve. This theorem is the same in both macro and
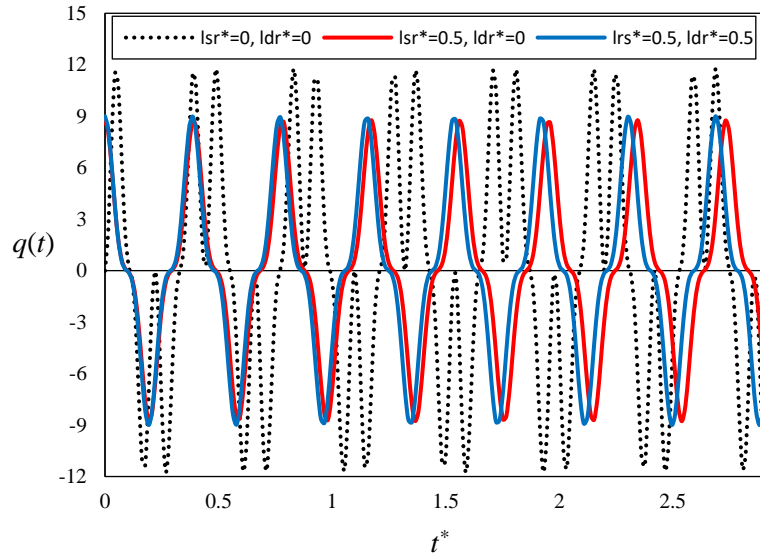
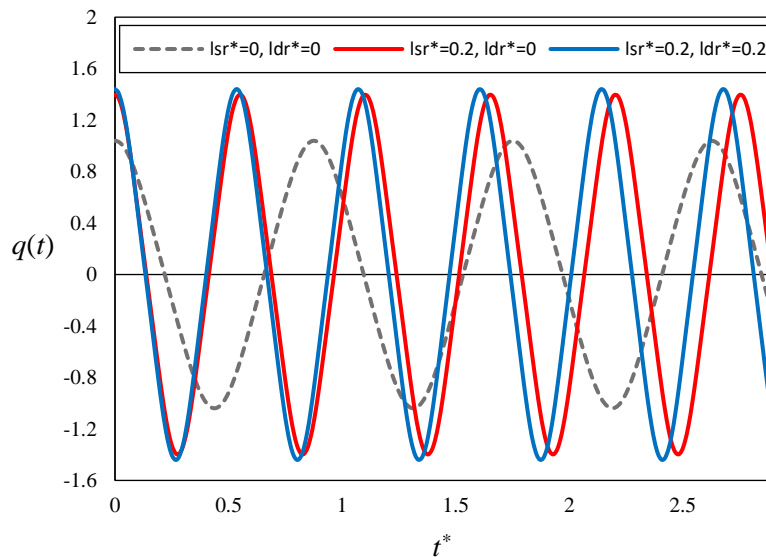microscale conditions, and it has nothing to do with scale effect and can be given as a general result.
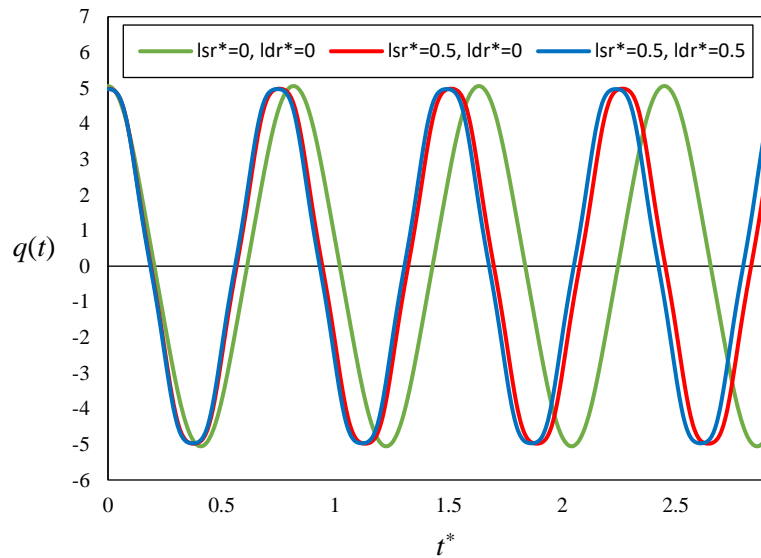
Fig 9a. Time response vs. large frequency amplitude
including $L^*=10, f^*=0.5, m=1$, SS.
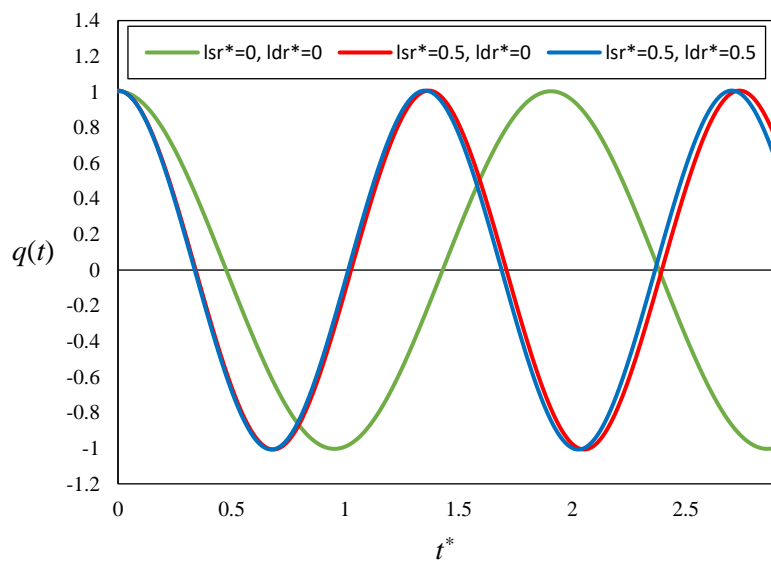
Fig 9b. Time response vs. small frequency amplitude
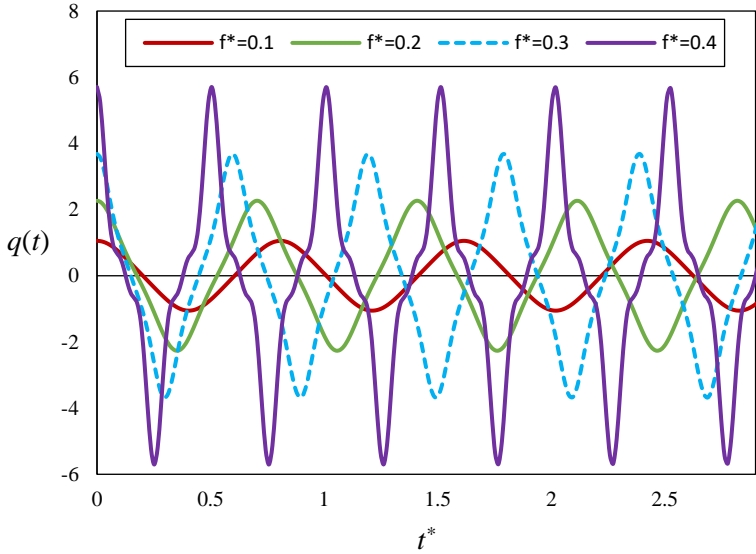including $L^*=10, f^*=0.1, m=1$, SS.

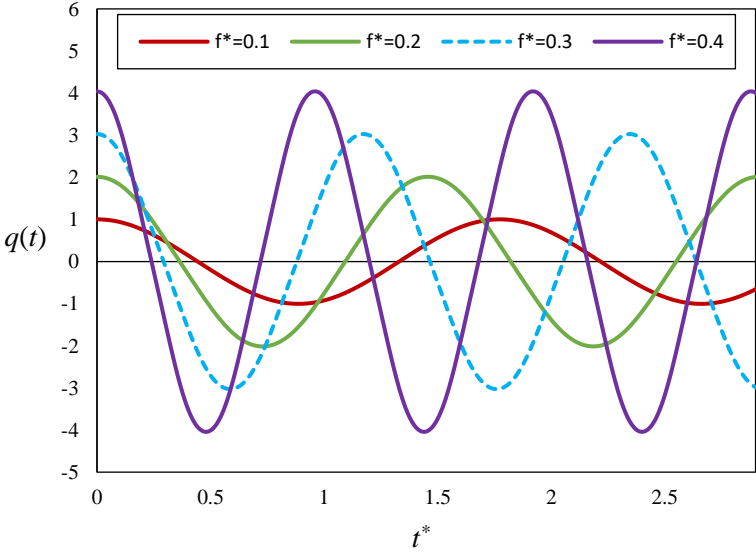**Fig 10a.** Time response vs. large frequency amplitude including $L^*=10, f^*=0.5, m=1$, CC.

Fig 10b. Time response vs. small frequency amplitude including $L^*=10, f^*=0.1, m=1$, CC.

As the last part of the study, Figures 11a and 11b are drawn out to reveal the effect of the frequency domain on the time response of the vibrating system. Figure 11a is dedicated to the two ends-clamped boundary conditions and Figure 11b is associated with the two ends-hinged boundary conditions. As it is vivid, in the hinged boundary condition, ascending the frequency amplitude leads to a growth in the number of motion cycles only and consequently to an increase in the frequency itself. But in Figure 11a, the result is different, and in the double-fixed ended beam, when the frequency amplitude is getting larger, the shape of the time

response also changes. The interesting thing to note in this figure is that when the beam crosses the allowed region of linear analysis, the response of the system varies. For the clamp boundary condition, linear analysis usually gives correct results until the transverse deflection is approximately 10-20 percent of the thickness (of course, it differs depending on several conditions). As one can see, from $f^*=0.2$, a change in the system response is appearing. Physically, the system goes through chaos from the harmonic state. Therefore, when the beam is doubly clamped, and the frequency amplitudes are in the range of nonlinear analysis, the nonlinear frequency study is requestable.

Fig 11a. Time response vs. frequency amplitudes including $L^*=10$, $l_{sr}^*=0.2$, $l_{dr}^*=0.2$, $m=1$, CC.

Fig 11b. Time response vs. frequency amplitudes

including $L^*=10$, $l_{sr}{}^*=0.2$, $l_{dr}{}^*=0.2$, $m=1$, SS.

7 Conclusions

The purpose of the choice of the current title was in light of two critical problems which have hardly ever been addressed in the literature. The researchers used to study the mechanics of microstructures on the basis of couple stress theories without taking into account any dynamic part inside the couple stress models. Most of the available literature included a static part for the micro-rotations only. But, here, we have studied the modified version of couple stress theory involving the dynamic effect of micro-rotations, namely micro-mass inertias. We assumed that this property could influence the mechanical response of a microstructure subject to dynamic conditions. Hence, we have engaged both static (SLS) and dynamic length scale parameters (DLS) in the couple stress model and showed that the DLS is really needful in some conditions. In addition to this, large amplitude and nonlinear natural frequencies have been investigated by establishing an analytical two-step process based on the Galerkin separation method and then the Homotopy perturbation technique to find out the time-dependent frequency response of the supposed micro-beam. According to the approximate analytical procedure, the obtained equation, which characterizes the large-amplitude frequency response of the beam, has been transformed into an ODE and thereafter solved with some routine mathematical operations. The solution process has also been verified by comparing the results with those of the FEM and a fairly good agreement has been witnessed. Our observations provide some new points presented as,

*The greater the frequency amplitude, the higher the nonlinear natural frequencies.
*The importance of the study of nonlinear frequency becomes remarkable when both SLS and DLS are getting bigger.
*The higher the frequency amplitude, the different the time response of the clamped beam.
*The greater the amount of SLS, the further meaningful the DLS.
*Micro-mass inertia causes stiffness hardening into the material.
*The increase in values of DLS similar to the SLS makes the material stiffer; however, the second parameter is more capable to differ the structural response.
*The microstructural effect varies the time response of materials leading to phase difference.
*The micro-mass inertia is becoming a vital factor when time goes higher.
*The time history of vibrations could be different for large amplitude frequencies compared to small amplitudes.

*Large amplitude-frequency analysis can be seriously required for clamped beams in both macro and micro scales.

Appendix A

Inserting Eq. (81) into Eq. (82) leads to,

$$\begin{cases} C_1'(t)\cos(\lambda_1 t) + C_2'(t)\sin(\lambda_1 t) = 0 \\ \\ C_1'(t)\left[\cos(\lambda_1 t)\right]' + C_2'(t)\left[\sin(\lambda_1 t)\right]' = \\ -\left(\lambda_1 f - f\omega^2 + \frac{3}{4}\lambda_2 f^3\right)\cos(\omega t) - \frac{1}{4}\lambda_2 f^3 \cos(3\omega t) \end{cases} \qquad \text{(A-1,2)}$$

If we rearrange Eq. (A-1) based on the C_1, then put it into Eq. (A-2),

$$-\left(-C_2'(t)\frac{\sin(\lambda_1 t)}{\cos(\lambda_1 t)}\right)\lambda_1\sin(\lambda_1 t) + \lambda_1 C_2'(t)\cos(\lambda_1 t) = -\left(\lambda_1 f - f\omega^2 + \frac{3}{4}\lambda_2 f^3\right)\cos(\omega t)$$

$$-\frac{1}{4}\lambda_2 f^3 \cos(3\omega t) \qquad \text{(A-3)}$$

From Eq. (A-3) one can obtain C_2 as,

$$C_1'(t) = \left(\lambda_1 f - f\omega^2 + \frac{3}{4}\lambda_2 f^3\right)\int\left[\sin(\lambda_1 t)\cos(\omega t)\right]dt + \frac{1}{4}\lambda_2 f^3\int\left[\sin(\lambda_1 t)\cos(3\omega t)\right]dt \qquad \text{(A-4)}$$

And respectively C_1 as,

$$C_2'(t) = -\left(\lambda_1 f - f\omega^2 + \frac{3}{4}\lambda_2 f^3\right)\int\left[\cos(\lambda_1 t)\cos(\omega t)\right]dt$$

$$-\frac{1}{4}\lambda_2 f^3\int\left[\cos(\lambda_1 t)\cos(3\omega t)\right]dt \qquad \text{(A-5)}$$

The solution of integrals existed in Eqs. (A-4) and (A-5) can be seen below,

$$\int\left[\sin(\lambda_1 t)\cos(\omega t)\right]dt = -\frac{\omega\sin(\omega t)\sin(\lambda_1 t) + \lambda_1\cos(\omega t)\cos(\lambda_1 t)}{\omega^2 - \lambda_1^2}$$

$$\int\left[\sin(\lambda_1 t)\cos(3\omega t)\right]dt = -\frac{3\omega\sin(3\omega t)\sin(\lambda_1 t) + \lambda_1\cos(3\omega t)\cos(\lambda_1 t)}{9\omega^2 - \lambda_1^2}$$

$$\int \left[\cos(\lambda_1 t) \cos(\omega t) \right] dt = \frac{\omega \cos(\omega t) \sin(\lambda_1 t) - \lambda_1 \cos(\omega t) \sin(\lambda_1 t)}{\omega^2 - \lambda_1^2}$$

$$\int \left[\cos(\lambda_1 t) \cos(3\omega t) \right] dt = \frac{3\omega \cos(3\omega t) \sin(\lambda_1 t) - \lambda_1 \cos(3\omega t) \sin(\lambda_1 t)}{9\omega^2 - \lambda_1^2}$$

Finally,

$$\Rightarrow C_1(t) = -\left(\lambda_1 f - f\omega^2 + \frac{3}{4}\lambda_2 f^3 \right)\left(\frac{\omega \sin(\omega t)\sin(\lambda_1 t) + \lambda_1 \cos(\omega t)\cos(\lambda_1 t)}{\omega^2 - \lambda_1^2} \right)$$
$$-\frac{1}{4}\lambda_2 f^3 \left(\frac{3\omega \sin(3\omega t)\sin(\lambda_1 t) + \lambda_1 \cos(3\omega t)\cos(\lambda_1 t)}{9\omega^2 - \lambda_1^2} \right)$$

(A-6)

$$\Rightarrow C_2(t) = -\left(\lambda_1 f - f\omega^2 + \frac{3}{4}\lambda_2 f^3 \right)\left(\frac{\omega \cos(\omega t)\sin(\lambda_1 t) - \lambda_1 \cos(\omega t)\sin(\lambda_1 t)}{\omega^2 - \lambda_1^2} \right)$$
$$-\frac{1}{4}\lambda_2 f^3 \left(\frac{3\omega \cos(3\omega t)\sin(\lambda_1 t) - \lambda_1 \cos(3\omega t)\sin(\lambda_1 t)}{9\omega^2 - \lambda_1^2} \right)$$

(A-7)

Here, using Eqs. (A-6) and (A-7) one receives,

$$q_1(t) = -\left[\left(\lambda_1 f - f\omega^2 + \frac{3}{4}\lambda_2 f^3 \right)\left(\frac{\omega \sin(\omega t)\sin(\lambda_1 t) + \lambda_1 \cos(\omega t)\cos(\lambda_1 t)}{\omega^2 - \lambda_1^2} \right) \right.$$
$$\left. -\frac{1}{4}\lambda_2 f^3 \left(\frac{3\omega \sin(3\omega t)\sin(\lambda_1 t) + \lambda_1 \cos(3\omega t)\cos(\lambda_1 t)}{9\omega^2 - \lambda_1^2} \right) \right]\cos(\lambda_1 t) +$$
$$\left[-\left(\lambda_1 f - f\omega^2 + \frac{3}{4}\lambda_2 f^3 \right)\left(\frac{\omega \cos(\omega t)\sin(\lambda_1 t) - \lambda_1 \cos(\omega t)\sin(\lambda_1 t)}{\omega^2 - \lambda_1^2} \right) \right.$$
$$\left. -\frac{1}{4}\lambda_2 f^3 \left(\frac{3\omega \cos(3\omega t)\sin(\lambda_1 t) - \lambda_1 \cos(3\omega t)\sin(\lambda_1 t)}{9\omega^2 - \lambda_1^2} \right) \right]\sin(\lambda_1 t)$$

(A-8)

On the basis of the initial conditions mentioned by Eq. (72), one derives

$$q_1(t) = f\left(\lambda_1 - \omega^2 + \frac{3}{4}f^2\lambda_2 \right)\left(\frac{\lambda_1}{\omega^2 - \lambda_1^2} \right)\cos(\omega t) + \frac{f^3\lambda_2}{4}\left(\frac{\lambda_1}{9\omega^2 - \lambda_1^2} \right)\cos(3\omega t)$$
$$+\left[f\left(\lambda_1 - \omega^2 + \frac{3}{4}f^2\lambda_2 \right)\left(\frac{\lambda_1}{\lambda_1^2 - \omega^2} \right) + \frac{f^3\lambda_2}{4}\left(\frac{\lambda_1}{\lambda_1^2 - 9\omega^2} \right) \right]\cos(\lambda_1 t)$$

(A-9)

It should be said that these processes will be redone for q_2. By doing so, one derives

$$q_2(t) = \left\{ 3\lambda_2 f^3\left(\lambda_1 - \omega^2 + \frac{3}{4}f^2\lambda_2\right)\left(\frac{\lambda_1}{\omega^2 - \lambda_1^2}\right)\left\{ -\frac{3}{4}\frac{\left(\begin{array}{c}\omega\sin(\omega t)\sin(\lambda_1 t)\\ +\lambda_1\cos(\omega t)\cos(\lambda_1 t)\end{array}\right)}{\omega^2 - \lambda_1^2} - \frac{1}{4}\frac{\left(\begin{array}{c}3\omega\sin(3\omega t)\sin(\lambda_1 t)\\ +\lambda_1\cos(3\omega t)\cos(\lambda_1 t)\end{array}\right)}{9\omega^2 - \lambda_1^2} \right\} \right.$$

$$+ \frac{3}{4}f^5\lambda_2^2\left(\frac{\lambda_1}{9\omega^2 - \lambda_1^2}\right)\left\{ -\frac{1}{4}\frac{\left(\begin{array}{c}\omega\sin(\omega t)\sin(\lambda_1 t)\\ +\lambda_1\cos(\omega t)\cos(\lambda_1 t)\end{array}\right)}{\omega^2 - \lambda_1^2} - \frac{1}{2}\frac{\left(\begin{array}{c}3\omega\sin(3\omega t)\sin(\lambda_1 t)\\ +\lambda_1\cos(3\omega t)\cos(\lambda_1 t)\end{array}\right)}{9\omega^2 - \lambda_1^2} - \frac{1}{4}\frac{\left(\begin{array}{c}5\omega\sin(5\omega t)\sin(\lambda_1 t)\\ +\lambda_1\cos(5\omega t)\cos(\lambda_1 t)\end{array}\right)}{25\omega^2 - \lambda_1^2} \right\} +$$

$$\left. \left[3\lambda_2 f^3\left(\lambda_1 - \omega^2 + \frac{3}{4}f^2\lambda_2\right)\left(\frac{\lambda_1}{\lambda_1^2 - \omega^2}\right) + \frac{3}{4}f^5\lambda_2^2\left(\frac{\lambda_1}{\lambda_1^2 - 9\omega^2}\right)\right]\left\{ -\frac{1}{8}\frac{\left(\begin{array}{c}\omega\sin(2\omega t)\sin(2\lambda_1 t)\\ +\lambda_1\cos(2\omega t)\cos(2\lambda_1 t)\end{array}\right)}{\omega^2 - \lambda_1^2} - \frac{1}{8}\frac{\cos(2\lambda_1 t)}{\lambda_1} \right\} \right\}\cos(\lambda_1 t)$$

$$
+\left\{
\begin{aligned}
&-3\lambda_2 f^3\left(\lambda_1-\omega^2+\frac{3}{4}f^2\lambda_2\right)\left(\frac{\lambda_1}{\omega^2-\lambda_1^2}\right)\left\{\frac{3}{4}\frac{\binom{\lambda_1\cos(\omega t)\sin(\lambda_1 t)}{-\omega\sin(\omega t)\cos(\lambda_1 t)}}{\omega^2-\lambda_1^2}+\frac{1}{4}\frac{\binom{\lambda_1\cos(3\omega t)\sin(\lambda_1 t)}{-3\omega\sin(3\omega t)\cos(\lambda_1 t)}}{9\omega^2-\lambda_1^2}\right\}\\[4pt]
&-\frac{3}{4}f^5\lambda_2^2\left(\frac{\lambda_1}{9\omega^2-\lambda_1^2}\right)\left\{\frac{1}{4}\frac{\lambda_1\cos(\omega t)\sin(\lambda_1 t)-\omega\sin(\omega t)\cos(\lambda_1 t)}{\omega^2-\lambda_1^2}+\frac{1}{2}\frac{\lambda_1\cos(3\omega t)\sin(\lambda_1 t)-3\omega\sin(3\omega t)\cos(\lambda_1 t)}{9\omega^2-\lambda_1^2}+\frac{1}{4}\frac{\lambda_1\cos(5\omega t)\sin(\lambda_1 t)-5\omega\sin(5\omega t)\cos(\lambda_1 t)}{25\omega^2-\lambda_1^2}\right\}\\[4pt]
&-\left[3\lambda_2 f^3\left(\lambda_1-\omega^2+\frac{3}{4}f^2\lambda_2\right)\left(\frac{\lambda_1}{\lambda_1^2-\omega^2}\right)+\frac{3}{4}f^5\lambda_2^2\left(\frac{\lambda_1}{\lambda_1^2-9\omega^2}\right)\right]\left\{\frac{1}{8}\frac{\binom{\lambda_1\cos(2\omega t)\sin(2\lambda_1 t)}{-\omega\sin(2\omega t)\cos(2\lambda_1 t)}}{\omega^2-\lambda_1^2}+\frac{1}{8}\frac{\sin(2\omega t)}{\omega}+\frac{1}{8}\frac{\sin(2\lambda_1 t)}{\lambda_1}+\frac{1}{4}\lambda_1\right\}
\end{aligned}
\right\}\sin(\lambda_1 t)
$$

$$\text{(A-10)}$$

And based on Eq. (74) and the separation of secular terms, the nonlinear natural frequency will be attained. Then, the q_2 is acquired as follows,

$$
q_2(t)=
$$
$$
\left\{
\begin{aligned}
&\frac{3}{4}f^3\lambda_2\left(\lambda_1-\omega^2+\frac{3}{4}f^2\lambda_2\right)\left(\frac{\lambda_1}{\omega^2-\lambda_1^2}\right)\left(3\frac{\lambda_1}{\omega^2-\lambda_1^2}+\frac{\lambda_1}{9\omega^2-\lambda_1^2}\right)\cos(\omega t)\\[4pt]
&+\frac{3}{16}f^5\lambda_2^2\left(\frac{\lambda_1}{9\omega^2-\lambda_1^2}\right)\left(\frac{\lambda_1}{\omega^2-\lambda_1^2}+2\frac{\lambda_1}{9\omega^2-\lambda_1^2}+\frac{\lambda_1}{25\omega^2-\lambda_1^2}\right)\cos(3\omega t)
\end{aligned}
\right\}\cos^2(\omega t)
$$
$$
+\left\{
\begin{aligned}
&\frac{3}{4}f^3\lambda_2\left(\lambda_1-\omega^2+\frac{3}{4}f^2\lambda_2\right)\left(\frac{\lambda_1}{\omega^2-\lambda_1^2}\right)\left(3\frac{\lambda_1}{\lambda_1^2-\omega^2}+\frac{\lambda_1}{\lambda_1^2-9\omega^2}\right)\\[4pt]
&+\frac{3}{16}f^5\lambda_2^2\left(\frac{\lambda_1}{9\omega^2-\lambda_1^2}\right)\left(\frac{\lambda_1}{\lambda_1^2-\omega^2}+2\frac{\lambda_1}{\lambda_1^2-9\omega^2}+\frac{\lambda_1}{\lambda_1^2-25\omega^2}\right)\\[4pt]
&+\frac{1}{8}\left[3f^3\lambda_2\left(\lambda_1-\omega^2+\frac{3}{4}f^2\lambda_2\right)\left(\frac{\lambda_1}{\lambda_1^2-\omega^2}\right)+\frac{3f^5\lambda_2^2}{4}\left(\frac{\lambda_1}{\lambda_1^2-9\omega^2}\right)\right]\left(\frac{\lambda_1}{\lambda_1^2-\omega^2}\right)
\end{aligned}
\right\}\cos(\lambda_1 t)
$$

The general time response of the system can be drawn using Eq. (66).

Reference

Abdul-Majid, W. (2011). *Linear and Nonlinear Integral Equations: Methods and Applications*. Springer Heidelberg Dordrecht, London. New York.

Abdussalam Nuhu, A., Safaei, B. (2022). A comprehensive review on the vibration analyses of small-scaled plate-based structures by utilizing the nonclassical continuum elasticity theories. *Thin-Walled Structures*, *179*, Article 109622.

Akbarzadeh Khorshidi, M. (2018). The material length scale parameter used in couple stress theories is not a material constant. *International Journal of Engineering Science*, *133*, 15-25.

Anthoine, A. (2000). Effect of couple-stresses on the elastic bending of beams. *International Journal of Solids and Structures*, *37*, 1003-1018.

Arefi, M., Taghavian, S. H. (2022). Dynamic characteristics of composite micro lattice plates comprises of graphene nanoplatelets based on MCST theory. *Thin-Walled Structures*, *175*, Article 109200.

Barretta, R., Čanađija, M., Luciano, R., de Sciarra, F. M. (2022). On the mechanics of nanobeams on nano-foundations. *International Journal of Engineering Science*, *180*, Article 103747.

Bhashyam, G., Prathap, G. (1980). Galerkin finite element method for non-linear beam vibrations. *Journal of Sound and Vibration*, *72*, 191-203.

Chen, S. X., Sahmani, S., Safaei, B. (2021). Size-dependent nonlinear bending behavior of porous FGM quasi-3D microplates with a central cutout based on nonlocal strain gradient isogeometric finite element modelling. *Engineering with Computers*, *37*, 1657–1678.

Chen, W., Yan, Zh., Wang, L. (2020). On mechanics of functionally graded hard-magnetic soft beams. *International Journal of Engineering Science*, *157*, Article 103391.

Darban, H., Luciano, R., Basista, M. (2022). Free transverse vibrations of nanobeams with multiple cracks. *International Journal of Engineering Science*, *177*, Article 103703.

Darban, H., Fabbrocino, F., Luciano, R. (2020). Size-dependent linear elastic fracture of nanobeams. *International Journal of Engineering Science*, *157*, Article 103381.

Dastjerdi, Sh., Akgöz, B., Civalek, Ö., Malikan, M., Eremeyev, V. A. (2020). On the non-linear dynamics of torus-shaped and cylindrical shell structures. *International Journal of Engineering Science*, *156*, Article 103371.

Dastjerdi, Sh., Malikan, M., Akgöz, B., Civalek, Ö., Wiczenbach, T., Eremeyev, V. A. (2022). On the deformation and frequency analyses of SARS-CoV-2 at nanoscale. *International Journal of Engineering Science*, *170*, Article 103604.

Dastjerdi, Sh., Naeijian, F., Akgöz, B., Civalek, Ö. (2021). On the mechanical analysis of microcrystalline cellulose sheets. *International Journal of Engineering Science*, *166*, Article 103500.

Dehrouyeh-Semnani, A. M. (2021). On large deformation and stability of microcantilevers under follower load. *International Journal of Engineering Science*, *168*, Article 103549.

Dehrouyeh-Semnani, A. M. Mostafaei, H. (2021). On the mechanics of microshells of revolution. *International Journal of Engineering Science*, *161*, Article 103450.

Eringen, A. C. (1999). *Microcontinuum Field Theory. I. Foundations and Solids*, Springer, New York.

Fan, F., Cai, X., Sahmani, S., Safaei, B. (2021). Isogeometric thermal postbuckling analysis of porous FGM quasi-3D nanoplates having cutouts with different shapes based upon surface stress elasticity. *Composite Structures*, 262, Article 113604.

Fathalilou, M., Sadeghi, M., Rezazadeh, Gh. (2014). Micro-inertia effects on the dynamic characteristics of micro-beams considering the couple stress theory. *Mechanics Research Communications*, *60*, 74-80.

Georgiadis, H. G., Velgaki, E. G. (2003). High-frequency Rayleigh waves in materials with micro-structure and couple-stress effects. *International Journal of Solids and Structures*, 40, 2501-2520.

Grekova, E. F. (2019). Nonlinear isotropic elastic reduced and full Cosserat media: waves and instabilities. *Continuum Mechanics and Thermodynamics*, *31*, 1805–1824.

Hadjesfandiari, A. R., Dargush, G. F. (2015). *Foundations of consistent couple stress theory*. https://doi.org/10.48550/arXiv.1509.06299

He, J.-H. (1999). Homotopy perturbation technique. *Computer Methods in Applied Mechanics and Engineering*, *178*, 257-262.

He, D., Yang, W., Chen, W. (2017). A size-dependent composite laminated skew plate model based on a new modified couple stress theory. *Acta Mechanica Solida Sinica*, *30*, 75-86.

Jouneghani, F. Z., Babamoradi, H., Dimitri, R., Tornabene, F. (2020). A Modified Couple Stress Elasticity for Non-Uniform Composite Laminated Beams Based on the Ritz Formulation. *Molecules*, *25*, Article 1404.

Karami, B., Janghorban, M., Fahham, H. (2022). On the stress analysis of anisotropic curved panels. *International Journal of Engineering Science*, *172*, Article 103625.

Kong, S. (2022). A Review on the Size-Dependent Models of Micro-beam and Micro-plate Based on the Modified Couple Stress Theory. *Archives of Computational Methods in Engineering*, *29*, 1–31.

Kumar Jena, S., Chakraverty, S., Mahesh, V., Harursampath, D. (2022). Application of Haar wavelet discretization and differential quadrature methods for free vibration of functionally graded micro-beam with porosity using modified couple stress theory. *Engineering Analysis with Boundary Elements*, *140*, 167-185.

Lai, M., Ruben, D., Krempl, E. (1993). *Introduction to Continuum Mechanics*. Pergamon Press, Oxford.

Li, Zh., He, Y., Lei, J., Guo, S., Liu, D., Wang, L. (2018). A standard experimental method for determining the material length scale based on modified couple stress theory. *International Journal of Mechanical Sciences*, *141*, 198-205.

Lu, L., She, G.-L., Guo, X. (2021). Size-dependent postbuckling analysis of graphene reinforced composite microtubes with geometrical imperfection. *International Journal of Mechanical Sciences*, *199*, Article 106428.

Ma, Y., Gao, Y., Yang, W., He, D. (2020). Free vibration of a micro-scale composite laminated Reddy plate using a finite element method based on the new modified couple stress theory. *Results in Physics*, 16, Article 102903.

Malikan, M. (2017). Electro-mechanical shear buckling of piezoelectric nanoplate using modified couple stress theory based on simplified first order shear deformation theory. *Applied Mathematical Modelling*, *48*, 196-207.

Malikan, M., Eremeyev, V. A. (2021). Flexomagnetic response of buckled piezomagnetic composite nanoplates. *Composite Structures*, *267*, Article 113932.

Malikan, M., Eremeyev, V. A. (2022). On a flexomagnetic behavior of composite structures, *International Journal of Engineering Science*, *175*, Article 103671.

Malikan, M., Krasheninnikov, M., Eremeyev, V. A. (2020a). Torsional stability capacity of a nano-composite shell based on a nonlocal strain gradient shell model under a three-dimensional magnetic field. *International Journal of Engineering Science*, *148*, Article 103210.

Malikan, M., Uglov, N. S., Eremeyev, V. A. (2020b). On instabilities and post-buckling of piezomagnetic and flexomagnetic nanostructures. *International Journal of Engineering Science*, *157*, Article 103395.

Mindlin, R. D. (1963). Influence of couple-stresses on stress concentrations. *Experimental Mechanics*, *3*, 1–7.

Mindlin, R. D., Tiersten, H. F. (1962). Effects of couple-stresses in linear elasticity. *Archive for Rational Mechanics and Analysis*, *11*, 415–448.

Qu, Y. L., Li, P., Zhang, G. Y., Jin, F., Gao, X.-L. (2020). A microstructure-dependent anisotropic magneto-electro-elastic Mindlin plate model based on an extended modified couple stress theory. *Acta Mechanica*, *231*, 4323–4350.

Russillo, A. F., Failla, G., Alotta, G., de Sciarra, F. M., Barretta, R. (2021). On the dynamics of nano-frames. *International Journal of Engineering Science*, *160*, Article 103433.

Russillo, A. F., Failla, G., Barretta, R., de Sciarra, F. M. (2022). On the dynamics of 3D nonlocal solids. *International Journal of Engineering Science*, *180*, Article 103742.

Safaei, B. (2021). Frequency-dependent damped vibrations of multifunctional foam plates sandwiched and integrated by composite faces. *European physical journal plus*, *136*, Article 646.

Sedighi, H. M., Bozorgmehri, A. (2016). Dynamic instability analysis of doubly clamped cylindrical nanowires in the presence of Casimir attraction and surface effects using modified couple stress theory. *Acta Mechanica*, *227*, 1575–1591.

Shariati, M., Azizi, B., Hosseini, M., Shishesaz, M. (2021). On the calibration of size parameters related to non-classical continuum theories using molecular dynamics simulations. *International Journal of Engineering Science*, *168*, Article 103544.

Sobamowo, M. G., Yinusa, A. A., Popoola, O. P., Waheed, M. A. (2021). Nonlinear Vibration Analysis of Thermo-Magneto-Mechanical Piezoelectric Nanobeam Embedded in Multi-Layer Elastic Media based on Nonlocal Elasticity Theory. *Journal of Materials and Engineering Structures*, *8*, 373–402.

Stempin, P., Sumelka, W. (2022). Space-fractional small-strain plasticity model for microbeams including grain size effect. *International Journal of Engineering Science*, *175*, 103672.

Thanh, C.-L., Tran, L. V., Vu-Huu, T. (2019). M. Abdel-Wahab, The size-dependent thermal bending and buckling analyses of composite laminate microplate based on new modified couple stress theory and isogeometric analysis. *Computer Methods in Applied Mechanics and Engineering*, 350, 337-361.

Toupin, R. A. (1962). Elastic materials with couple-stresses. *Archive for Rational Mechanics and Analysis*, *11*, 385–414.

Tsiatas, G. C. (2009). A new Kirchhoff plate model based on a modified couple stress theory. *International Journal of Solids and Structures*, *46*, 2757-2764.

Wang, Y.-G., Lin, W.-H., Liu, N. (2012). A Homotopy Perturbation-Based Method for Large Deflection of a Cantilever Beam Under a Terminal Follower Force. *International Journal for Computational Methods in Engineering Science and Mechanics*, *13*, 197-201.

Wang, L., Zheng, Sh. (2018). Nonlinear analysis of 0–3 polarized PLZT microplate based on the new modified couple stress theory. *Physica E: Low-dimensional Systems and Nanostructures*, *96*, 94-101.

Xu, X., Karami, B., Shahsavari, D. (2021a). Time-dependent behavior of porous curved nanobeam. *International Journal of Engineering Science*, *160*, Article 103455.

Xu, X., Shahsavari, D., Karami, B. (2021b). On the forced mechanics of doubly-curved nanoshell. *International Journal of Engineering Science*, *168*, Article 103538.

Yang, F., Chong, A. C. M., Lam, D. C. C., Tong, P. (2002). Couple stress based strain gradient theory for elasticity. *International Journal of Solids and Structures*, *39*, 2731-2743.

Yang, Sh., Chen, W. (2015). On hypotheses of composite laminated plates based on new modified couple stress theory. *Composite Structures*, *133*, 46-53.

Yang, Z., Lu, H., Sahmani, S., Safaei, B. (2021). Isogeometric couple stress continuum-based linear and nonlinear flexural responses of functionally graded composite microplates with variable thickness. *Archives of Civil and Mechanical Engineering*, *21*, Article 114.

Yuan, Y., Zhao, K., Zhao, Y., Sahmani, S., Safaei, B. (2020). Couple stress-based nonlinear buckling analysis of hydrostatic pressurized functionally graded composite conical microshells. *Mechanics of Materials*, *148*, Article 103507.

Zum Gahr, K.-H. (1987). *Microstructure and Wear of Materials*. Tribology Series, Elsevier.